Wood and Resin Composite Extrusion for Additive Manufacturing

A Thesis
Presented in Partial Fulfillment of the Requirements for the
Degree of Master of Science
with a
Major in Mechanical Engineering
in the
College of Graduate Studies
University of Idaho
by

Conal S. Thie

Major Professor: Michael Maughan, Ph.D., PE
Co-Major Professor: Tao Xing, Ph.D., PE
Committee Members: Armando McDonald, Ph.D.; Kenneth Baker, M.Arch.
Department Administrator: Gabriel Potirniche, Ph.D., PE

August 2021

Authorization to Submit Thesis

This thesis of Conal S. Thie, submitted for the degree of Master of Science with a Major in Mechanical Engineering and titled "Wood and Resin Composite Extrusion for Additive Manufacturing," has been reviewed in final form. Permission, as indicated by the signatures and dates below, is now granted to submit final copies to the College of Graduate Studies for approval.

Major Professor:	_____ Michael Maughan, Ph.D., PE	Date: _____
Co-Major Professor:	_____ Tao Xing, Ph.D., PE	Date: _____
Committee Members:	_____ Armando McDonald, Ph.D	Date: _____
	_____ Kenneth Baker, M.Arch.	Date: _____
Department Administrator:	_____ Gabriel Potirniche, Ph.D., PE	Date: _____

Abstract

Additive manufacturing is a quickly growing manufacturing technique with a multitude of applications. It has the ability to rapidly manufacturing geometries that other techniques cannot. Additionally, it produces very little waste material and can use recycled materials. Additive manufacturing is becoming popular in the building construction industry. Currently, concrete is the primary additive manufacturing material being used in the construction industry. Wood-based composites have yet to be used in additive manufacturing for the construction industry because a method to use high wood content composites in additive manufacturing has not been developed. This study details the development of a wood-based composite extrusions method for additive manufacturing.

A screw extruder was designed and constructed that could extrude wood-based composites with high wood content. This extruder produced many composite samples of various wood element sizes and resin content that were then cured. The cured sample sets were tested using a 3-point bend test. Samples were oven cured at different temperatures and time periods. It was determined that the rate at which the samples were cured did not affect the bending properties of the composite. For a sample made with wood element size less than 40 mesh and cured for two days at 50°C, the bending strength and modulus of elasticity were 24.7 MPa and 4.6 GPa respectively. These mechanical properties are relatively close to OSB and fiber board. Thus, the extruded wood-based composites are suitable to replace traditional composites based on strength and modulus performance.

Capillary rheology was performed to test the properties of the wood-based composite during extrusion. A custom capillary rheometer was designed and fabricated to perform these tests. The viscosity of the composite was found to be non-Newtonian and shear-thinning. A power-law model was used to characterize the viscosity. The power-law model was then used in a CFD model to simulate the capillary rheology extrusion. The CFD model was able to simulate the extrusion pressure of the capillary rheometer within 1.6% error, compared to the experimental value.

Acknowledgements

Thank you to my major and co-major professors, Dr. Michael Maughan and Dr. Tao Xing, for their support and guidance throughout my graduate education. I would like to thank Dr. Armando McDonald for his advice and aid while working in his lab. I wish to express my gratitude to Ken Baker for his leadership on this project, as well as his support. Thank you to all my fellow graduate students who I had the pleasure of working with over the last two years. Finally, I would like to acknowledge the state of Idaho's Higher Education Research Council for funding this project through the Idaho Global Entrepreneurial Mission (IGEM) Grant Program.

Dedication

I would like to dedicate this thesis to my mother and my father. I am incredibly grateful for the love and support they have given me throughout my education.

Table of Contents

List of Tables

List of Figures

Chapter 1: Introduction

Extrusion based additive manufacturing is a rapidly growing industry with a vast range of applications. One of the most novel of these applications is in the construction industry. In 2019 the market for 3D printing in construction had an estimated market size of $3 million and has been projected to reach over $1.5 billion by 2024 [1]. There are a multitude of drivers for 3D printing in construction including mass customization, new architectural features, reduced safety risks for workers, reduced waste, and sustainability.

Additive manufacturing has primarily been done with polymers. However, recently there has been an increase of different materials being used in additive manufacturing. Development in using metals, foams, concrete, and composites for 3D printing has emerged. In the construction industry, concrete has often been the material of choice for additive manufacturing. Companies such as XtreeE, CyBe, and Apis Cor have been using concrete material to manufacturing houses and other large scale projects using layer-by-layer additive manufacturing. One of the reasons concrete materials dominate the 3D printing construction market is because of their flowability. When in their liquid state, concretes are easily extruded. While using concrete materials does have advantages in large scale 3D printing, one untapped material in this industry is wood. Lumber is a cornerstone in the construction industry, yet wood-based composites have had little exploration in additive manufacturing.

Wood-based composites have the potential to expand the 3D printing construction market tremendously. Introducing a new sustainable material into this market will expand it. Furthermore, using wood-based composites in large scale additive manufacturing has more benefits. A common advantage in all additive manufacturing is waste reduction. The amount of scrap material produced in 3D printing is miniscule when compared to traditional manufacturing methods. Using wood-based composites builds on this advantage by using waste-wood from other industries, making it the most sustainable material option. The ability to reuse scrap material gives wood-based composites an advantage over concrete in the 3D printing construction industry. To make a wood-based composite as sustainable as possible requires it to be composed a high concentration of waste wood. However, extruding dry waste wood is a difficult process. Unlike wet concrete, dry, wood-based composites do not flow easily. Before wood-based composites can be utilized in the construction industry this challenge must be solved. The purpose of this research was to begin the methodology of a process able to cold print building assembles using waste wood elements. The final outcome of the research is to develop a reliable process for 3D printing house walls, floors, and roofs on a horizontal printing bed. This process can then be used to manufacture modular residential homes for low cost.

This study presents the development of a method to extrude wood-based composites for the purpose of additive manufacturing in the construction industry. In addition, bending strength of the material was tested, and the flow of the composite was examined experimentally and computationally.

Chapter 2: Background and Literature Review

2.1 Additive Manufacturing

3D printing is expanding from just prototyping and molds to consumer products and architectural structures. Early additive manufacturing industries include aerospace, automotive and healthcare. The potential to 3D-print entire buildings has recently gained attention. This is due to the potential to decrease labor costs, reduce waste, and fabricate complex geometries [2]. Construction 3D printing is currently being dominated by concrete extrusion; however, the forest and construction industries are researching how large-scale wood-based 3D printing can be made possible. Wood slurries have been a popular method to attempt wood-based additive manufacturing on the large scale. Unfortunately, there are many difficulties with wood slurries including: poor rheology for the application especially with high solid content, inability to layer and bind, and nozzle clogging due to premature material solidification. Regardless, the demand for wood-based 3D-printing is growing [3].

Many wood-based composites used in additive manufacturing have less than 50% wood weight content. Due to the low wood content, they have a higher adhesive content, which is expense. These composites are used in small scale 3D printing, rather than the large-scale construction industry. Figure 2-1 illustrates the scale of one of these smaller-scale processes [4]. In this case, the composite had a 30:70 wood to PLA weight ratio. The average cost PLA is almost ten times that of the sawdust [4]. Because of this cost disparity, to make wood-based 3D printing possible on the larger scale, the amount of wood content in the composite must be increased.

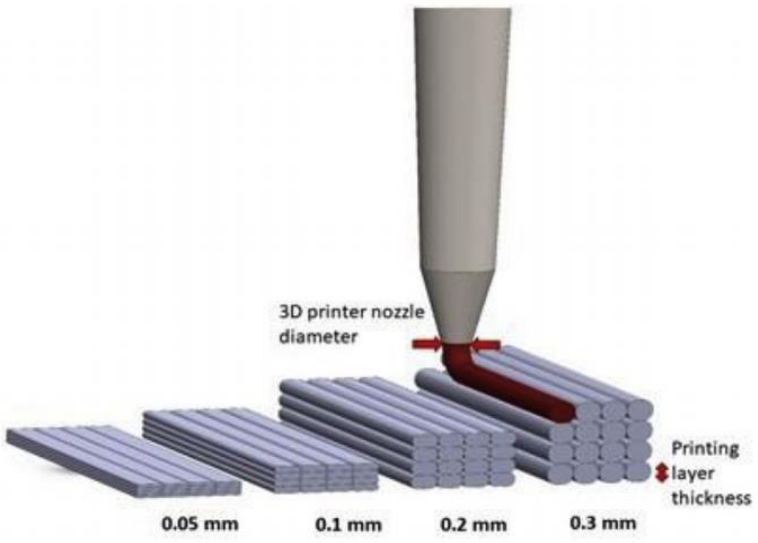

Figure 2-1: Small Scale 3D Printing Process [4]

A novel approach to wood-based additive manufacturing is individual layer fabrication [5]. This process entails laminating individual wood layers with an adhesive, and then pressing them together. Due to the added mechanical pressure in this process, the amount of adhesive used can be reduced relative the other wood-based composites. Figure 2-2 displays how this process operates. One downside of this process, compared to traditional 3D printing, is that each layer must be pressed individually. This could limit the manufacturing speed and geometric flexibility which traditional 3D printing has.

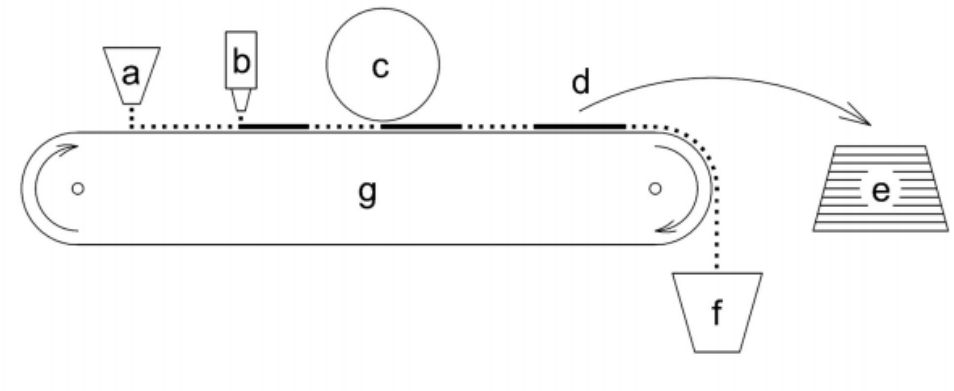

Figure 2-2: Individual layer fabrication method [5]
(a) Dispensing of Bulk, (b) Fluid Application, (c) Pressing, (d) Contoured panel, (e) Solid Object Formed by Laminated Panels, (f) Removal of Unbound Material, (g) conveying of work pieces.

Powder bed processes are those which use powder as an additive material. There are multiple forms of this type of process. Generally, powder is added to a bed layer-by-layer by a roller or wiping blade [6]. The layers are fused together with a heat source or binder. Parts formed by powder bed processing are characteristically porous, unless the powder layers are heated to a melting point. Figure 2-3 depicts one of these melting powder bed processes [7]. In the depicted process a blade is used to wipe the powder from the dispenser platform onto the build platform. A laser is used to fuse the powder layers together.

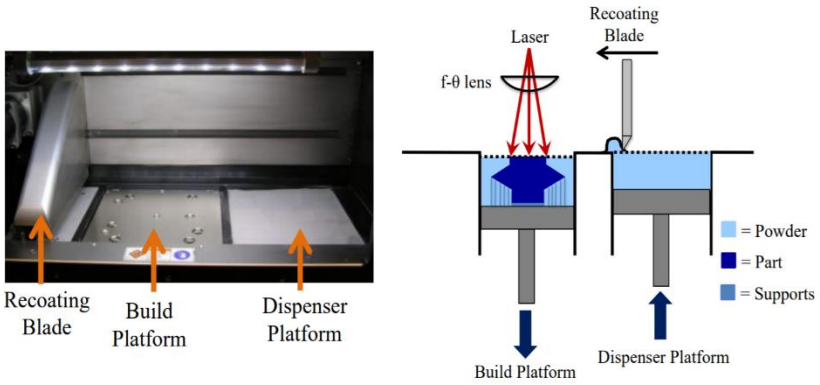

Figure 2-3: Laser heated powder bed process [7].

2.2 Rheology

Rheology is the science which studies material flow under applied stresses. Rheology can be applied to many different materials, including those which are elastic, viscous, and viscoelastic [8]. Rheometry is the experimental techniques for measuring the rheology of materials. One common form of rheometry is done with a capillary rheometer. Typically, a capillary rheometer consists of a barrel, plunger, heater, die, and sensors. Shear stress is induced by the plunger pushing the material through the narrow die. Heaters are used to melt the material and test how temperature effects the flow. Figure 2-4 illustrates the characteristic components of a capillary rheometer.

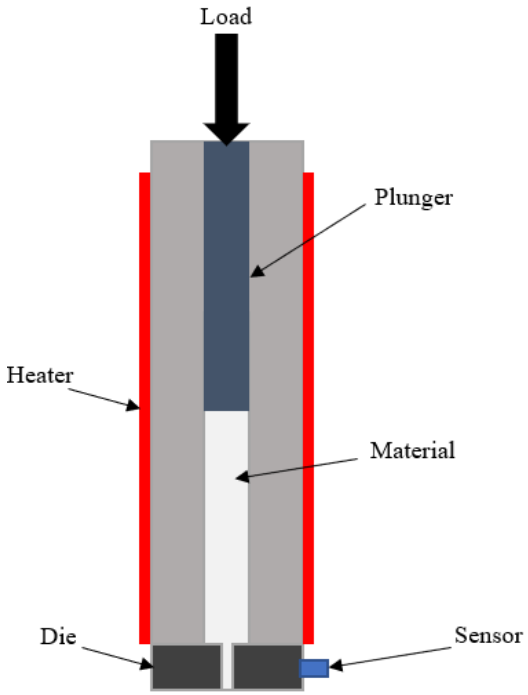

Figure 2-4: Capillary rheometer schematic.

More advanced custom rheometers are buildable to accommodate specific functions and testing. For example, Figure 2-4 is a capillary rheometer designed to perform direct pressure measurements inside the capillary die [9].

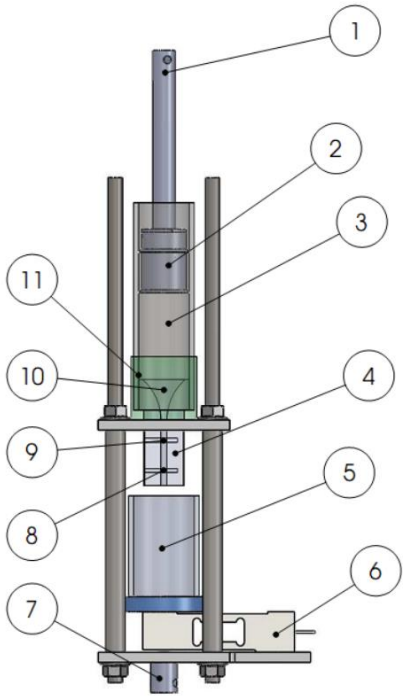

Figure 2-5: Custom capillary rheometer [9]
(1) RAM, (2) piston, (3) barrel, (4) capillary die, (5) feed collector, (6) load cell, (7) bottom connector, (8), (9) and (11) are the location of pressure measurements and (10) entry zone.

Wood-polymer rheology is possible to perform with capillary rheometry. When performing rheology on wood composites, wood content and species strongly influence the wall slip rate and viscosity [10]. The viscosity of the wood-polymer composites tends to increase as wood content increases. Influence of die geometry is also affected by species, for instance, pine has stronger dependence than maple. Additionally, in-line rheometry can be incorporated with 3D printing. By using specialized nozzles and sensors, pressures, temperatures, and viscosities within a 3D printing nozzle are measurable [11]. This allows for process control and real-time monitoring of critical measurements. Figure 2-5 illustrates a system design that can accomplish rheological 3D printing.

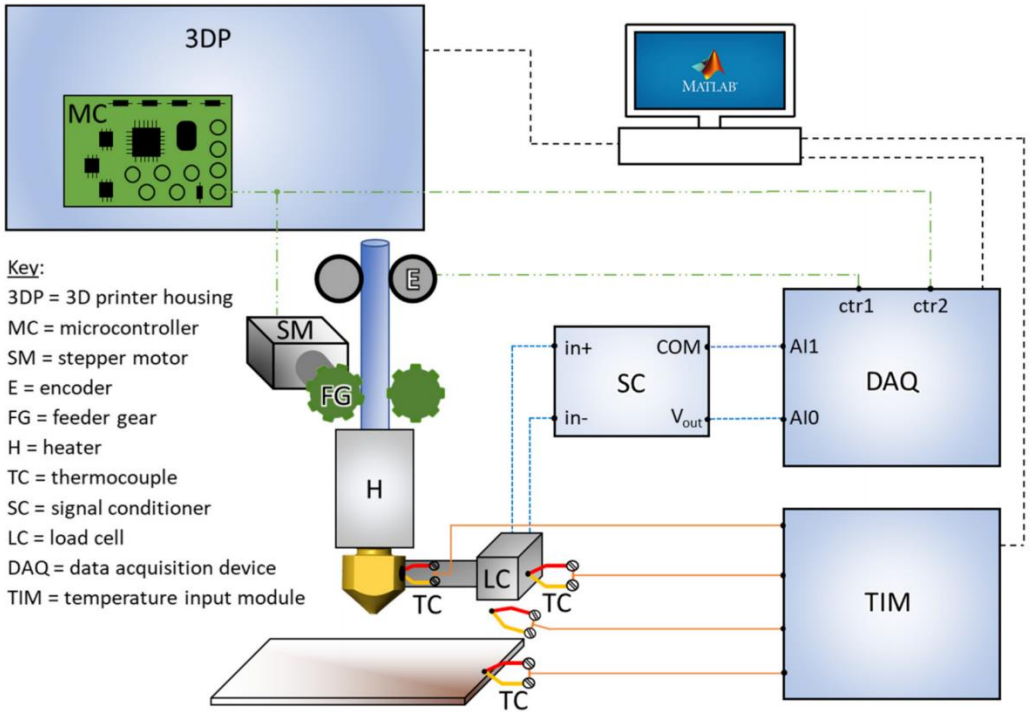

Figure 2-6: System of sensors, devices, and connections for in-line rheology and process monitoring [11].

2.3 CFD Modeling

Computational Fluid Dynamics (CFD) is a powerful simulation tool, which uses numerical analysis. CFD can be used to simulate a vast range of fluids and energy problems, including wind turbines, drying processes, bread baking, and capillary rheology [12-15]. ANSYS Fluent is an industry leading CFD software, which is commonly used in research. Fluent has useful tools to help simulate screw extrusion and capillary rheology, such as dynamic meshing and non-Newtonian viscosity models [16]. Dynamic meshing allows the mesh to deform and change throughout the simulation. This helps avert meshing errors that often prevent the simulation from working.

The continuity (1) and incompressible momentum (2) equations are the two governing equations for generic extrusion CFD simulations.

$$\nabla \cdot v = 0 \tag{1}$$

$$\frac{\partial v}{\partial t} = -\nabla \cdot p + \nabla \cdot \tau_{ij} \tag{2}$$

Where v is velocity, t is time, p is pressure, and τ is stress. Cylindrical extrusion simulations are efficiently done using an axisymmetric 2D model. These simulations are useful tools for improving die design parameters, such as taper angle, and outlet diameter [12]. Figure 2-6 displays a simple single nozzle extrusion model.

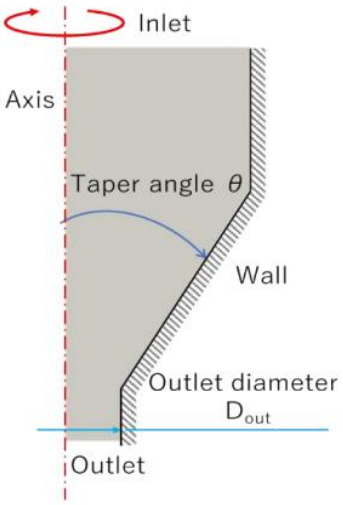

Figure 2-7: Single nozzle design for CFD simulation [12].

ANSYS Fluent provides the user with the ability to enter different non-Newtonian viscosity models into the simulation, including Power-Law, Carreau, Cross, and Herschel-Bulkley [16]. Using extrusion simulations, in conjunction with capillary rheometry experiments, allows for the creation of accurate viscosity modeling of polymers and composites.

2.4 Wood-Based Composite Materials

Wood-based composites are generally thought of as any wood-based material bonded together with an adhesive. Common wood-based composites in the construction industry are particle board, oriented strand board (OSB), and fiberboard [17]. These composites can be made from a variety of adhesives, element sizes, and wood species. Since these properties can all be controlled, wood-based composites are more consistent in performance than solid wood. Typically, the wood mass percentages is 94% or higher in these composites [17].

Thermosetting resins combined with a binder are the conventional adhesive. Thermosetting resins are those which are cured with heat. Common industry examples of these resin-binder couplings are phenol-formaldehyde (PF), urea-formaldehyde (UF), and melamine-formaldehyde (MF) [17]. Each resin has its own advantages and disadvantages. The factors to determine which resin to use include mechanical requirements, bonding time, wood species, and resin cost.

Wood element size often determines the type of final product produced. For example, OSB uses much larger wood elements than particle board. Element size also factors into product performance. Figure 2-7 shows the various element sizes used in wood composites. The static bending properties of common wood-based composites given in Table 2-1.

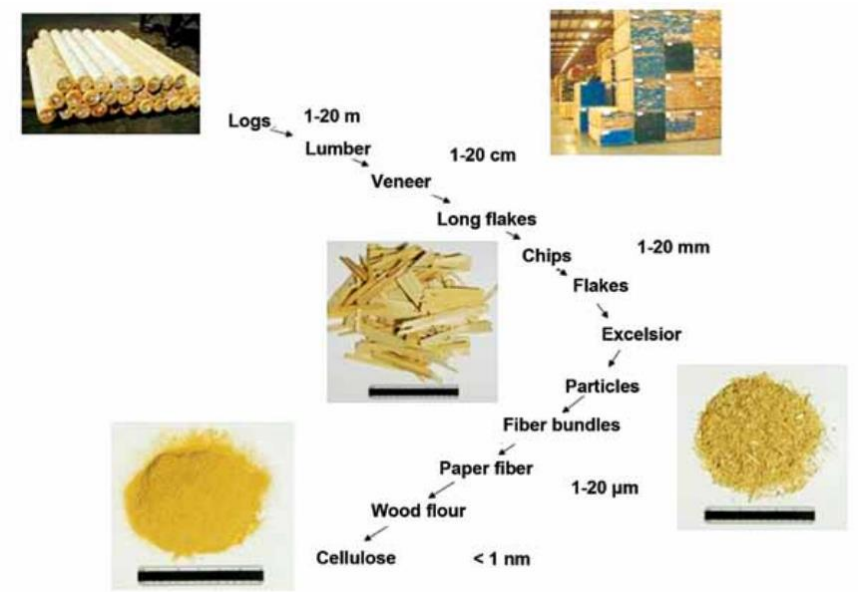

Figure 2-8: Wood element sizes, from largest to smallest [17].

Table 2-1: Static bending properties of common wood-based composites [17].

Material	Density (kg/m^3)	Modulus of Elasticity (GPa)	Bending Strength (MPa)
Medium Density Fiber Board	0.7-0.9	3.59	35.85
Particleboard	0.6-0.8	2.79-4.14	15.17-24.13
OSB	0.5-0.8	4.41-6.28	21.80-34.70

Static bending properties of wood-based composites are conventionally determined through 3-point static bend testing. The standard for these tests is described in ASTM D1037 [18].

Medium density fiber board (MDF) and particle board are both composed of two different types of layers. These two layers are face layers (`FL), which are on the outside of the board, and the core layer (CL) which is the middle layer. The density of these layers is highly influential to the strength properties of the board. MDF and particle board use high density face layers with low density core layers [19]. Figure 2-8 displays an example density profile of particle board. The face layers are denser than the core layer to increase strength performance while keeping the weight of the produce lower.

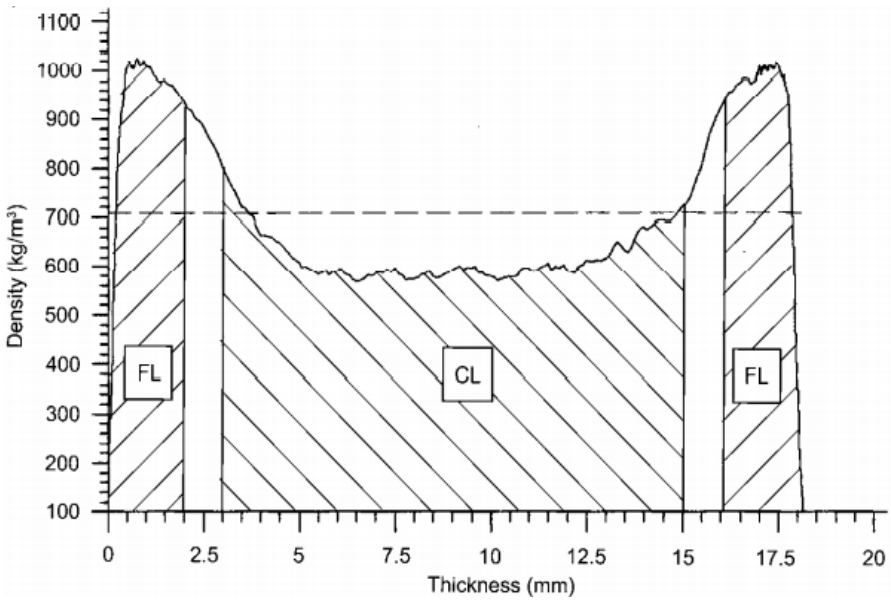

Figure 2-9: Density profile of particleboard [19].

Modulus of elasticity and bending strength are both considerably less in in the core layer than in the two face layers, Figure 2-9 shows these comparisons.

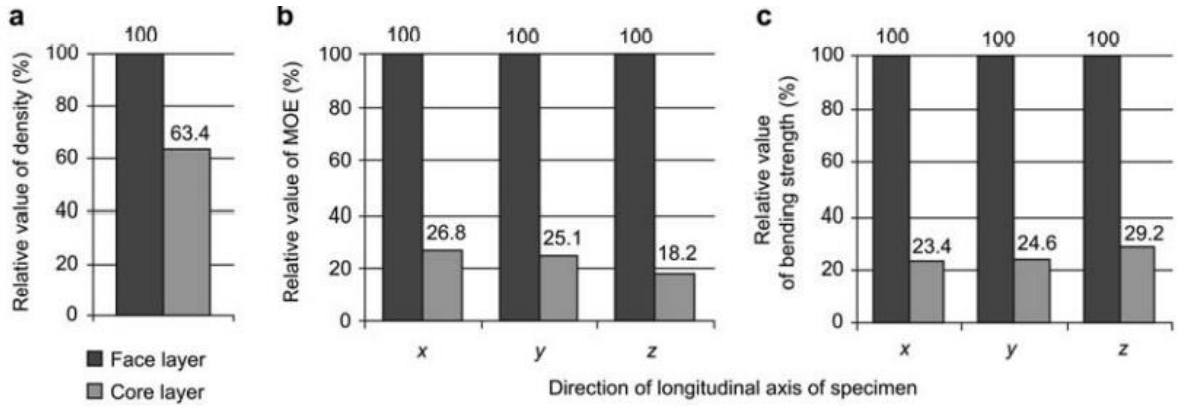

Figure 2-10: Comparison of density (a), modulus of elasticity (b) and bending strength (c) of particleboard layers [19].

Wood-based composite materials are affected by temperature, weathering, and moisture [20, 21]. As seen in Figure 2-10, particle board will decrease in strength as temperature increases.

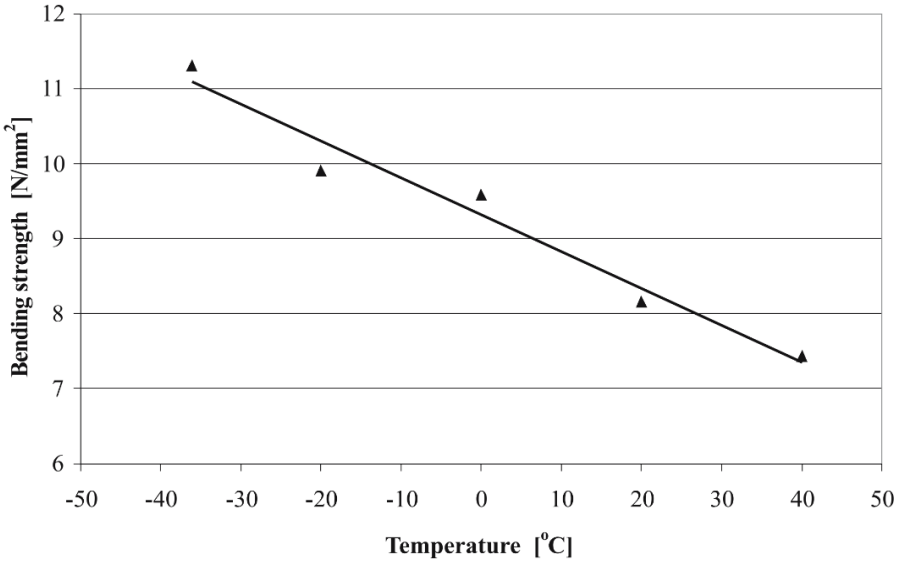

Figure 2-11: Influence of temperature on the bending strength of particleboards [20].

The modulus of elasticity of particle board also decreases as temperature increases. Weathering causes wood-based composites to decrease in both bending strength and modulus of elasticity as well. Controlling moisture in wood-based composites is vital in increasing weathering performance. Surface coatings, hydrophobic additives, and processing conditions are all effective moisture control method [21].

2.5 Screw Extrusion

Extrusion is any process in which a material, typically a fluid, is pumped through a die. The extrusion process is often continuous, which is ideal for efficient manufacturing. Screw extrusion is the most dominant type of continuous extrusion and is primarily used to extrude polymer melts [22]. The two most common types of screw extruders are single-screw and multi-screw. Single-screw extruders are the most common type of screw extruder for many reasons, including their ability to provide constant shear and their high throughput capabilities. Multi-screw extruders can be useful when processing materials which experience slipping on the barrel wall and they can provide better mixing, compared to single-screw extruders. The standard design for a single-screw extruder is illustrated in Figure 2-11.

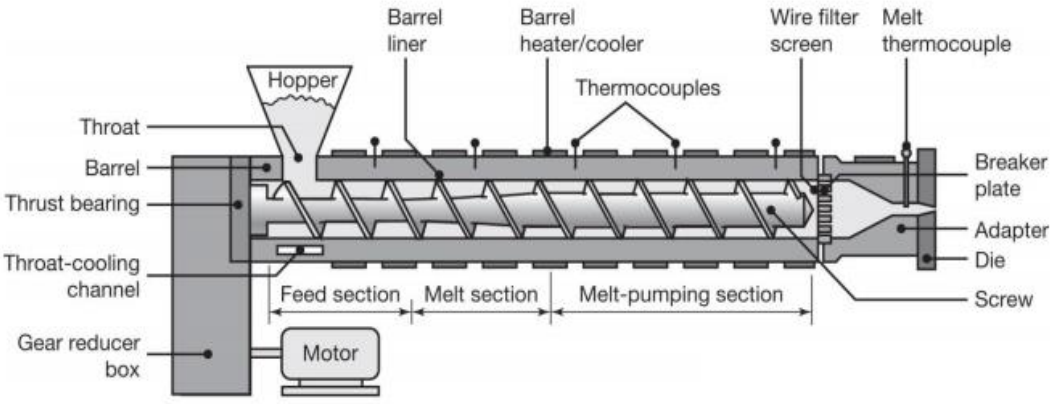

Figure 2-12: Standard single-screw extruder [6].

In the typical extrusion process for plastics, the hopper is filled with plastics in the form of pellets, granules, or powders. Plastic is pumped through the three sections of the extruder. These are the feed section, the melt or compression section, and the melt-pumping section. The screw begins to taper in the melt section, which causes the melting plastic to shear. Screw and die design play an important role in how the extruder functions. Figure 2-14 illustrates the basic design of an extrusion screw.

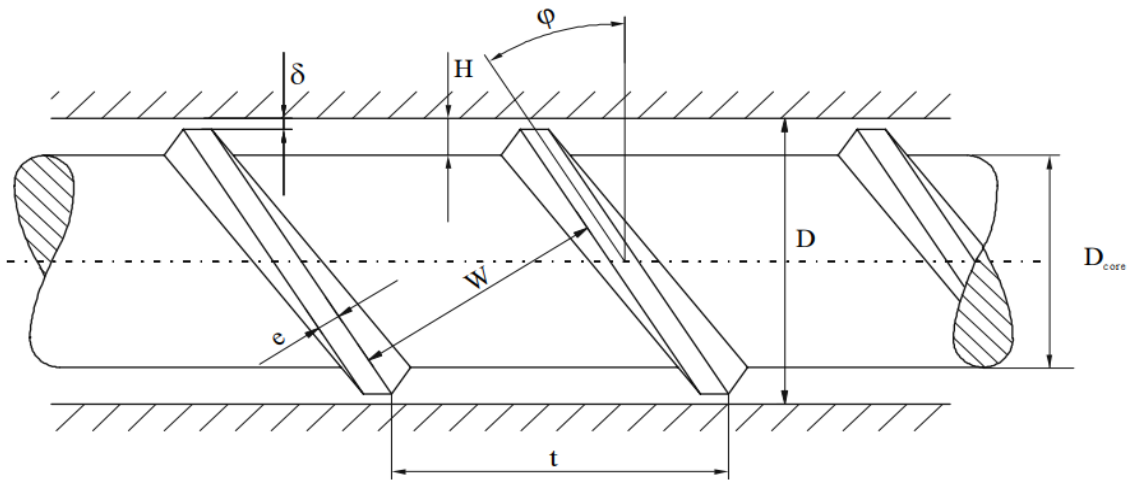

Figure 2-13: Screw geometry schematic [23].

The flow rate of the extruder while the pressure is constant in the pumping zone is known as the drag flow and is governed by the following equation:

$$Q_d = \frac{vHW}{2} \tag{3}$$

Where *v* is the flight velocity in the flow direction, *H* is the depth of the channel, and *W* is the width of the polymer. However, often the pressure in not constant in the pumping zone due to a build up of pressure at the die. Thus, the true pressure is given as:

$$Q_{extruder} = Q_d - Q_p \tag{4}$$

Where Q_p is the flow correction factor due to pressure [6]. For Newtonian fluids $Q_{extruder}$ can be written as:

$$Q_{extruder} = \frac{\pi^2 H D_{core}^2 sin\varphi cos\varphi}{2} - \frac{p\pi D_{core} H^3 sin^2\varphi}{12\eta L} \tag{5}$$

Where *p* is pressure, η is material viscosity, and *L* is the length of the pumping section. This equation is also known as the extruder characteristic [6].

Screw compression ratio is the ratio between the initial channel depth and the final channel depth. Typically, the compression ratio of a screw is between 1:2 and 1:4 [22]. The typical length-to-diameter ratio of a screw is between 20:1 to 30:1. High length-to-diameter ratios are important for uniform temperature control and pressure generation.

Die design is crucial to the extrusion process. The die provides compression and material shaping. Designs for dies are often developed from experimental testing. This is regularly done through capillary rheology. Figure 2-14 illustrates a simple die cross-section and the typical pressure

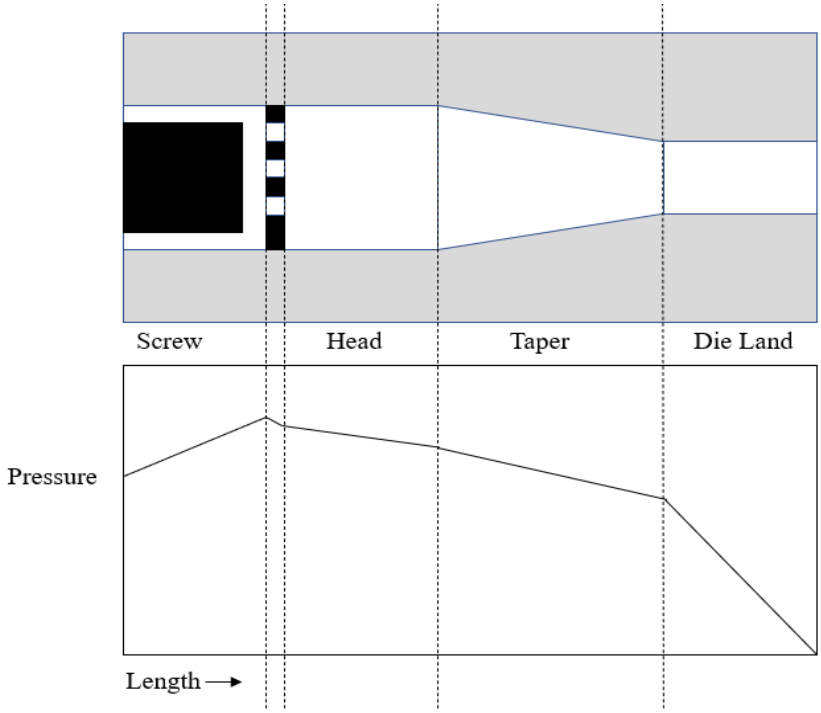

Figure 2-14: Simplified die cross-section compared to steady state pressure profile.

profile through the die. As shown, the pressure on the material begins to decrease once it enters the head of the die and eventually drops to zero at the die exit.

Die design effects the extrusion by inducing pressure to the flow. It is important to understand this process to optimize flow rate, material density and required motor torque. The general expression relating the flow and pressure inside the die is known as the die characteristic and is written as:

$$Q_{die} = Kp \tag{6}$$

Where Q_{die} is the flow through the die, p is the pressure at the die inlet, and K is a function of die geometry. Typically, K is determined experimentally, however, for circular die cross-sections there is a closed-form solution [6]. This equation is written as:

$$K = \frac{\pi D_d^4}{128 \eta L_d} \tag{7}$$

Where D_d is the diameter of the die-opening, and L_d is the length of the die land. If die and extruder characteristic equations are known, then the pressure and flow rate of the system can be solved algebraically.

When the material leaves the die, it does not typically retain the die's shape. Because the material is soft, and the die pressure is relieved, the material often swells. This is known as die swell. Die swell characteristically increases if any of the following happen: extrusion speed increases, die dimensions decrease, melt temperature decreases, or die land length to diameter ratio decreases [22].

The use of screw extrusion in 3D printing is historically uncommon. However, recently they have been used as a feeder in concrete 3D printing for wall construction [24]. As illustrated in Figure 2-15, a concrete 3D printer utilizes a screw and nozzle. Similar to polymer screw extruders, the screw in this system provides back pressure to push the concrete through the nozzle.

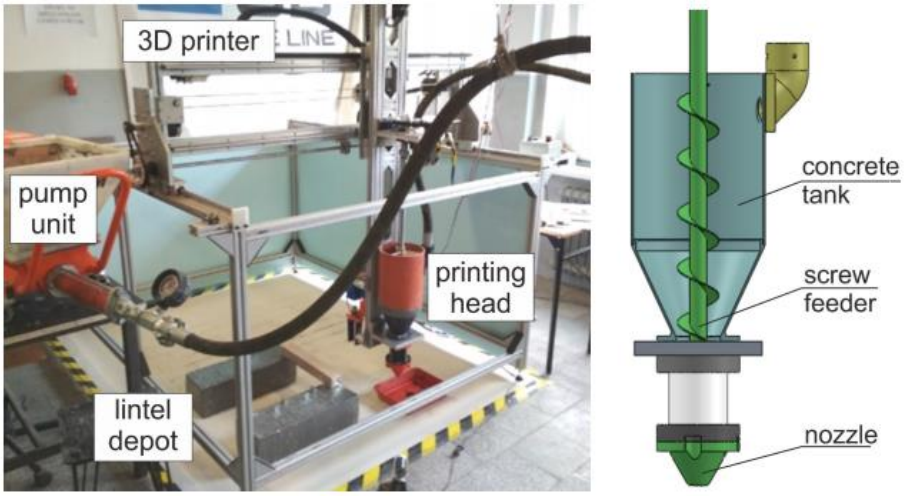

Figure 2-15: Concrete 3D printer with screw feeder [24].

2.6 Use of Wood in Buildings

Prior to the 20th century almost all commercial and residential buildings used wood as their primary building material. Both lumber and wood-based composites are still a primary building material today. Panel products, such as OSB and plywood, are frequently being used for sheathing, walls, and floors. This is due to their fast installation process and consistent structural properties [17].

One advantage wood has over most other building materials is its innate environmental benefits. Wood is a renewable resource with a low level of energy-based processing required. The amount of energy required to harvest, manufacture, and transport a material is known as its embodied energy [17]. Compared to other building materials such as, concrete, metal, or plastic, wood has the lowest embodied energy. Additionally, over half the energy used to manufacture wood products comes from bioenergy and, as seen in Table 2-2 [17], the amount of carbon emission produced by wood is substantially lower than other building materials.

Table 2-2: Net carbon emissions in producing a ton of various building materials [17].

Material	Net carbon emissions (kg C/t)[a,b]	Near-term net carbon emissions including carbon storage within material (kg C/t)[c,d]
Framing lumber	33	–457
Medium-density fiberboard (virgin fiber)	60	–382
Brick	88	88
Glass	154	154
Recycled steel (100% from scrap)	220	220
Concrete	265	265
Concrete[e]	291	291
Recycled aluminum (100% recycled content)	309	309
Steel (virgin)	694	694
Plastic	2,502	2,502
Aluminum (virgin)	4,532	4,532

[a]Values are based on life-cycle assessment and include gathering and processing of raw materials, primary and secondary processing, and transportation.
[b]Source: EPA (2006).
[c]From Bowyer and others (2008); a carbon content of 49% is assumed for wood.
[d]The carbon stored within wood will eventually be emitted back to the atmosphere at the end of the useful life of the wood product.
[e]Derived based on EPA value for concrete and consideration of additional steps involved in making blocks.

Chapter 3: Methods

Multiple extrusion methods were explored in this study, including screw extrusion and capillary rheology. Due to the novelty of wood-based composite extrusion, developments in the screw extrusion method had to be made before functional extrusions were possible. After the method for screw extrusion was developed, it was used to produce samples of the wood-based composite. These samples were examined using multiple methods. The wood-based composite was a mixture of fine wood flour and a thermoset resin. The ratio of wood flour to resin was a factor that was explored at length. Once extruded, the samples must dry for the resin to fully cure. Various curing and drying methods were performed on the extruded composite samples. Bending strength of the cured samples was tested using a 3-point bending method. Capillary rheology was performed primarily to gain an understanding of the composite while it is being extruded in a semi-fluid state. A numerical viscosity model of the composite was developed by using data from the rheology. This model was assessed in a Computational Fluid Dynamics (CFD) simulation.

3.1 Screw Extrusion for Wood Composites

The purpose of developing an extrusion method for wood-based composites is for its use in the construction additive manufacturing industry. Thus, the method must be compatible with additive manufacturing. Additive manufacturing requires the extrusion method to be continuous. Screw extrusion is a practical extrusion method that meets this requirement.

As seen in Figure 3-1, Wellzoom desktop filament extruder with a 3 mm die diameter was the initial testing device for this method.

Figure 3-1: Wellzoom desktop filament extruder.

This is a 150W screw extruder primarily meant for extruding PLA, ABS, and other plastics. Motor seizing and stalling occurred when used to extrude the wood-based composite. This was due to an insufficient motor for the application.

The second stage in developing an extrusion method for the composite was with a RobotDigg SJ35 screw extruder. As seen in Figure 3-2, the extruder has an inside barrel diameter of 35 mm and a 186.4 W (0.25 hp) motor.

Figure 3-2: RobotDigg SJ35 extruder.

The increase in barrel size compared to the Wellzoom extruder allows for larger extrusions, which are necessary for the scale of construction manufacturing. Many modification to the SJ35 extruder were required before it was fully operational. The first modification was a die modification. The die for the SJ35 was initially designed for thin plastic filament, not suitable for the larger wood extrusions. Thus, the die was modified by increasing the diameter and a second die was fabricated with an even larger die diameter. As seen in Figure 3-3, the large and small dies have diameters of 19 mm and 14 mm, respectively.

Figure 3-3: Large and small extruder dies.

The second modification made to the SJ35 extruder was to its screw. The initially delivered screw had a compression ratio of 7. This compression ratio was very high and caused unnecessary friction between the material and the barrel wall. When used to extrude melted plastic the friction is minor, but when used to extrude a wood-based composite the friction is increased. Due to this friction, the barrel heats up and motor is over worked. To fix this, a screw with a compression ratio of 1 was designed and fabricated. This screw drawing may be found in Appendix A. Since this screw does not compress the material, all the compaction is caused by the die. Both screws are steel and have a length to diameter ratio of 12:1. Figure 3-4 is a picture of the two screws.

Figure 3-4: High compression screw (top) zero compression screw (bottom).

The third modification made to the extruder was upgrading the motor. The original motor had a maximum speed of 16 RPM. Using the ideal motor torque equation:

$$T\ (lbf - ft) = \frac{Power\ (hp)\ * 33000}{2\pi * RPM} \quad (8)$$

the ideal torque the original motor provided was 111.3 N-m. It is important to note that the actual torque provided by this motor was lower than this ideal torque, due to inherent inefficiency in the system. Similar to the Wallzoom extruder, the original SJ35 extruder motor had stalling issues and would frequently overheat. Often what caused these issues was that the wood-based composite was too dry, the wood elements were too large, or the motor was being run at a high speed for too long. Thus, the motor was upgraded to a larger, higher power motor. The new motor is the NORD AC Gearmotor 230/460. This is a 745.7 W (1 hp) motor with an ideal torque of 178.0 N-m. The maximum speed of this motor is 40 RPM and it uses a gear ratio of 43.2:1.

The final modification made was adapting the new motor to the original barrel, screw, and frame. The NORD motor is much larger than the original motor, so a mounting plate had to be designed and fabricated to align the NORD motor with the original frame. Additionally, a shaft adapter was attached, and a new variable frequency drive (VFD) was installed. The new VFD is a Altivar 12. This is a 745.7 W AC drive with a single-phase input and a three-phase output. A VFD allowed for variable motor speeds and the ability to reverse the motor. After these modifications were made, wood-based extrusion was possible and the final stage in developing a screw extrusion method for wood-based composites was complete. Figure 3-5 shows the schematic of this system and Figure 3-6 is a picture of the operational system.

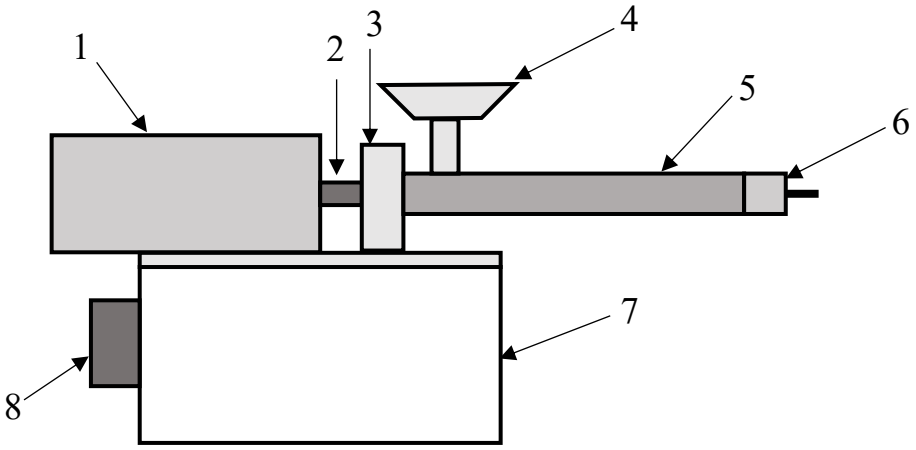

Figure 3-5: Schematic of final screw extruder
Items Listed: (1) NORD Motor, (2) Shaft Adapter, (3) Bearing Block, (4) Hopper, (5) Barrel, (6) Die, (7) Base, (8) VFD.
Not Shown: Screw.

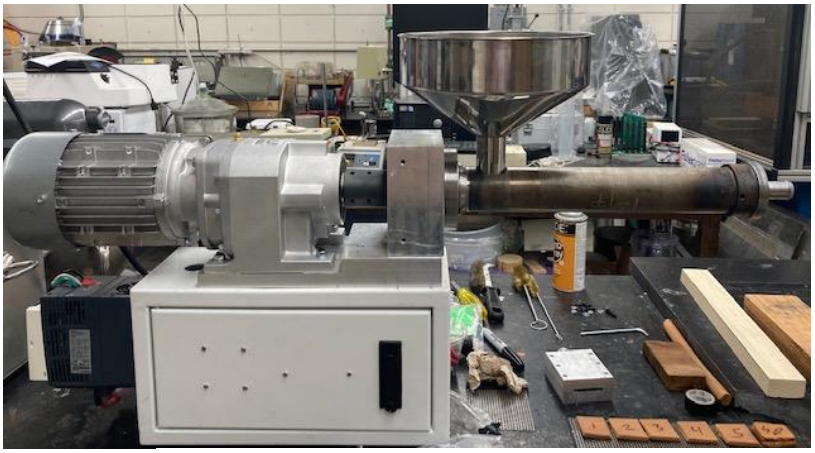

Figure 3-6: Picture of screw extruder system

The final system was used to extrude wood-based composite samples for strength and curing testing. As long as the hopper is filled, this system can extrude material continuously, and therefore can be used in additive manufacturing processes.

3.2 Wood-Based Composite Preparation and Testing

An important factor in how well the wood-based composite extrudes is the properties of the composite. Generally, the extruded composite is comprised of wood elements, an adhesive, and water. After extrusion, the water evaporates over time and the adhesive cures creating a dry, rigid sample. Different properties of the composite were varied and tested, including the size of the wood elements, ratio of wood to adhesive, and type of adhesive. How the extruded samples are dried and cured was also varied to test if the curing method influences the final sample.

The wood used was waste wood flour from Plummer Forest Products, Post Falls Idaho. It was sieved to separate element sizes. The primary element size used was flour which was less than 40 mesh (< 40), where 40 mesh is a standard US mesh that has a sieve size of 0.425 mm. The moisture content of the wood fiber was measured using a HB43-S Halogen Moisture Analyzer from Mettler Toledo, Columbus OH. The moisture content ranged between 5.8%-7%. The primary adhesive used was sodium silicate (Na_2O_3Si) from Thermo Fisher Scientific, Carlsbad, CA. Sodium silicate is a water-soluble thermoset resin. The sodium silicate solution was premixed with water at a weight ratio of 37% sodium silicate to 63% water. The wood-sodium silicate composite was mixed using a high torque food processor. The weight ratio of wood to sodium silicate was tested at different ratios including 40:60, 45:55, 50:50, and 60:40. To obtain a 50:50 weight ratio, 2.7 grams of the Fisher sodium silicate would be added for every 1 gram of wood to account for the premixed water.

After extrusion, the samples were placed in a drying tray and left to cure. Figure 3-7 shows the drying tray used. It is a wood tray with slots to allow for uniform drying, and to prevent samples from bowing. Samples were either placed in an oven at various temperatures or left at room temperature (22°C). The oven temperatures tested were 45°C, 50°C, 60°C, and 105°C. The curing time was 48 hours for samples cured in the oven and eleven days for samples cured at room temperature.

Figure 3-7: Samples curing on drying tray.

3.3 Rheology Frame and Die

Capillary rheology was performed as a preliminary extrusion method, as well as a tool to determine flow mechanics of the composite. A custom rheology frame, barrel, and die had to be designed and fabricated due to the scale of the extrusions. Figure 3-8 is the assembly diagram of the custom capillary rheometer.

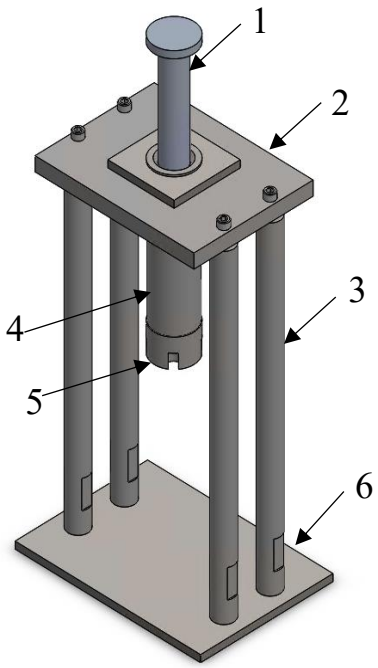

Figure 3-8: Diagram of custom rheology frame
Items Listed: (1) Plunger, (2) Top Plate, (3) Frame Leg,
(4) Barrel, (5) Capillary Die, (6) Base Plate.
Not Shown: Load cell.

The new frame, barrel, and die were designed to be used with an Instron 5500R-1137 universal testing machine, shown in Figure 3-10. This machine can be used for multiple purposes including tensile testing, bend testing, and capillary rheology. In addition to the designed components, a 133.4 kN (30,000 lbf) load cell was used. The rheometer is operated by first loading the barrel with the wood-based composite. Then, the crosshead is lowered at a constant rate, pushing the plunger into the barrel. As the plunger compresses the composite material inside the barrel, pressure increases. The resulting force on the load cell is measure using the software Bluehill 3. At a critical pressure point, the composite begins to flow through the exit die, resulting in an extruded product. The operating crosshead velocity of the load cell was varied. The key dimensions of the designed components are shown in Table 3-1.

Table 3-1: Primary part dimensions of custom capillary rheometer.

Part	Location	Dimension (mm)
Barrel	Inside Diameter	44.45
Barrel	Length	254.0
Plunger	Diameter	44.20
Plunger	Length	304.8

The final capillary rheometer design was fabricated in the University of Idaho machine shop. Once operational, the custom capillary rheometer was used to extrude samples and measure extrusion pressure for the purpose of developing a viscosity model of the wood-based composite. Figure 3-9 shows the final frame apparatus. Frame drawing may be found in Appendix B.

Figure 3-9: Custom rheology frame assembly.

3.4 Viscosity Model

A numerical model for the viscosity of the composite was developed to gain a better understanding of how the material flowed and to create a CFD simulation of the capillary rheology process. The composite model was designed to represent < 40 mesh element size, and with a wood to sodium silicate weight ratio of 50:50. A combined data set was used to create this model. This data set included data from dynamic rheology and capillary rheology. This section focuses on the method used to create the viscosity model using capillary rheology.

3.3.1 Experimental Data Collection

The capillary rheometer used was the custom rheometer designed and discussed in Section 3.2. The dimensions of the die used are those in Table 3-2, and the barrel dimensions are in Table 3-1.

Table 3-2: Capillary rheology die dimensions.

Location	**Dimension (mm)**
Diameter (*D'*)	8.89
Land Length *(L'*)	19.05
Taper Length	31.75

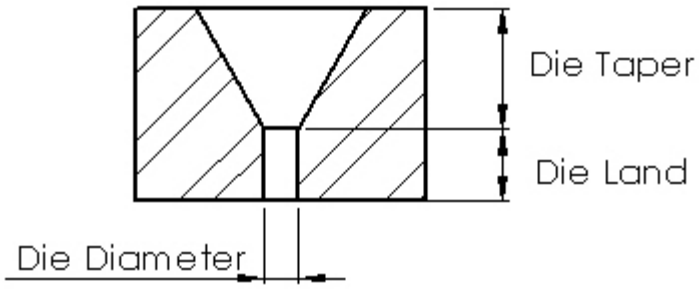

Figure 3-10: Cross-sectional view of rheology die.

Using the method described in ASTM Standard D3835 [25], true viscosity and true shear rate of the composite can be calculated using the following equations:

$$Q = \frac{V}{A} \tag{9}$$

$$P = \frac{F}{A} \tag{10}$$

$$\dot{\gamma}_a = \frac{32Q}{\pi D'^3} \tag{11}$$

$$\tau = \frac{PD'}{4L'} \tag{12}$$

$$\dot{\gamma} = \frac{3n+1}{4n}\dot{\gamma}_a \tag{13}$$

$$\eta = 10^6 \frac{\tau}{\dot{\gamma}} \tag{14}$$

Where:

F = force on crosshead during extrusion, N

P = pressure from crosshead during extrusion, Pa

V = crosshead velocity, mm/s

Q = volumetric flow rate, mm^3/s

A = cross-sectional area, mm^2

$\dot{\gamma}_a$ = apparent shear rate, 1/s

τ = shear stress, MPa

$\dot{\gamma}$ = true shear rate, 1/s

n = tangent slope of the log true shear stress versus log apparent shear rate curve, 0.3018

η = true viscosity, Pa*s

All extrusions were done at room temperature (21°C – 23°C) and the density of the compacted composite (ρ) was found after the extrusions were complete using the compacted composite left in the barrel. It was determined that the viscosity of the composite was shear-thinning and was modelled using the Power-Law model:

$$\eta = k\dot{\gamma}^{N-1} \tag{15}$$

Where k is the average viscosity of the fluid and N is the deviation of the fluid from a Newtonian form.

3.3.2 CFD Model

ANSYS Fluent 2020 R2 was used for simulating the flow of the composite during a capillary rheology extrusion. An axisymmetric model was used which included the die, and part of the barrel. The length of the barrel filled with composite was 235.0 mm and the total travel length of the plunger was 143.0 mm. These values were chosen to match a capillary rheology extrusion conducted at a crosshead velocity of 0.1667 mm/s. The simulation used an axisymmetric boundary condition, and a dynamic mesh was used to simulate the motion of the plunger. The dynamic mesh utilized the layering method. The general settings are shown in Table 3-3.

Table 3-3: CFD simulation settings.

Setting	Mode
Solver Type	Pressure Base
Time Solver	Transient
2D Space	Axisymmetric
Energy Model	Off
Viscous Model	Laminar
Time Step Size	0.05(s)
Max Iterations per Time Step	20
Absolute Criteria	0.0001
Scheme	SIMPLE
Gradient	Least Squares Cell Based
Pressure	Second Order
Momentum	Second Order Upwind

The simulation was executed with three different mesh element sizes for mesh verification. These element sizes were $1x10^{-3}$ m, $5x10^{-4}$ m and $2.5x10^{-4}$ m. Figure 3-13 shows the dimensions and boundary conditions of the simulation. The Plunger boundary condition was set as a no-slip wall. The wall boundary condition was set as both no-slip and specified shear stress in two different simulation variations. The outlet boundary condition was set as a zero-pressure outlet, and the axis of rotation boundary condition was set as axis.

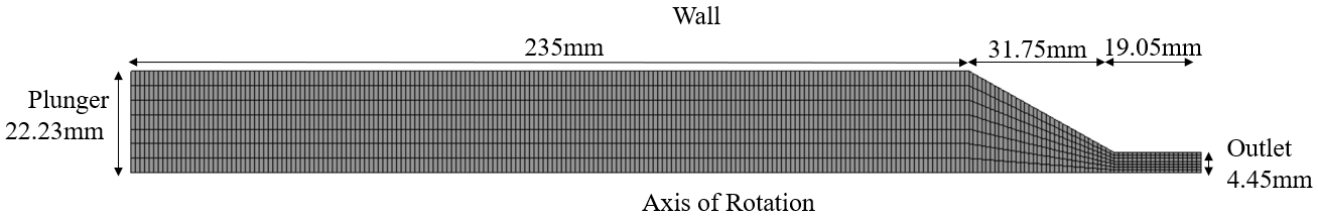

Figure 3-11: Simulation dimension and boundary condition with $1x10^{-3}$ m element size.

3.5 Bending Tests

To determine the bending strength of the cured composite samples, 3-point flexural bending tests were performed. The samples used were either cured in an oven or at room temperature. All samples were extruded using the custom screw extruder with a 14 mm die. Multiple sample parameters were varied to test their effects, including sample curing method, wood to sodium silicate weight ratio, and wood element size. Table 3-3 includes the list of sample sets tested. Each parameter was tested using a minimum of five replicates per sample set and a total of eight samples sets were tested.

Table 3-4: Bending Test Sample Sets

Sample Set #	Wood to Sodium Silicate Weight Ratio	Particle Mesh Size	Curing Method
1	50:50	< 40 mesh	1 day at 60°C 1 day at 105°C
2	50:50	< 40 mesh	2 days at 60°C
3	50:50	< 40 mesh	2 days at 50°C
4	50:50	< 40 mesh	2 days at 45°C
5	50:50	< 40 mesh	11 days at 22°C (Room Temp.)
6	55:45	< 40 mesh	2 days at 50°C
7	60:40	< 40 mesh	2 days at 50°C
8	50:50	20-40 mesh	2 days at 50°C

The testing system used was the Mecmesin MultiTest-dV 2.5. This is a modular force tester with multiple applications, including 3-point bend testing. The initial sample had a diameter of 13.5 mm; thus, a support span of 216 mm was used to apply a 1:16 diameter to span testing ratio. The diameter of the samples varied slightly, but the 216 mm span was kept consistent on every test. A continuous load was applied throughout the test at a constant downward velocity of 5 mm/min. The test was stopped when the sample broke. The load and deflection throughout the test were sampled by the machine. Flexural stress (σ_f) and flexural strain (ϵ_f) were calculated with the following equations:

$$\sigma_f = \frac{8FL}{\pi d^3} \tag{16}$$

$$\epsilon_f = \frac{600Dd}{L^2}(\%) \tag{17}$$

where F is the load on the sample (N), L is the support span (mm), d is the sample diameter (mm), and D is the deflect in the sample (mm). Figure 3-12 is a schematic of the 3-point bending test set-up and Figure 3-13 is a picture of the testing apparatus.

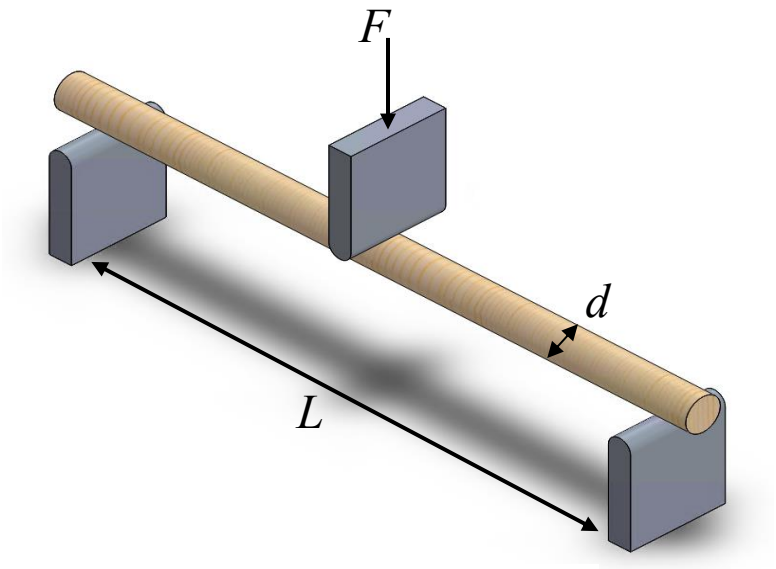

Figure 3-12: 3-Point bend test schematic.

Figure 3-13: Mecmesin MultiTest-dV; 3-point bending test configuration.

Chapter 4: Results

4.1 Characteristics of Extruded Products

When extruded with either the screw extruder or capillary rheometer the wood-resin composite extrudes as a damp, malleable, rod. Since the Fisher sodium silicate is premixed with water, the wetness of the extrudate depends on the wood to sodium silicate ratio. Typically, as the water content of the extrudate decreases the malleability decreases. Figure 4-1 is a picture of newly extruded composite from the screw extruder. The pictured composite had a 50:50 wood to sodium silicate weight ratio and used a wood element size of < 40 mesh.

Figure 4-1: Extrudate from screw extruder.

During extrusion, the extrudate would occasionally deform and crack on the outside. This phenomenon is known as the sharkskin effect. Figure 4-2 shows two examples of phenomenon in a wood-based composite. These samples were extruded using the screw extruder. When the sharkskin effect occurred, the extrusion was considered failed, and the composite samples were not used in further testing.

Figure 4-2: Sharkskin effect on wood-based composite.

Extruded composites with wood element size < 40 mesh typically had a smooth, uniform surface, as seen in Figure 4-1. However, extruded composites with larger wood element size of 20-40 mesh did not have a smooth uniform surface. These composites were craggy, with many cracks and a rough surface. Figure 4-3 is a picture of composite samples made with wood element size of 20-40 mesh and extruded with the screw extruder.

Figure 4-3: Extruded composite with wood element size of 20-40 mesh.

After extrusion, the composite began to dry and cure at a temperature dependent rate. Composite samples that were placed in an oven cured quicker than those that were dried at room temperature. During the curing process, the sodium silicate resin begins to solidify. Once fully cured, the composite is hard and rigid. The specific gravity of the cured samples is 0.7-0.9. Figure 4-4 pictures two hardened samples that were cured at room temperature. These samples had a 50:50 wood to sodium silicate weight ratio and used a wood particle size of < 40 mesh.

Figure 4-4: Cured wood-resin composite samples.

As the composite dries, surface cracking can occur. Table 4-1 lists how many composite samples cracked during drying, and the curing method being used. The samples listed in Table 4-1 had a 50:50 wood to sodium silicate weight ratio and used a wood particle size of < 40 mesh. Cracks were typically longitudinal and varied slightly in width and length. Figure 4-5 illustrates the variation of crack size.

Table 4-1: Cracking occurrences with respect to curing method.

Curing Method	Wood to Sodium Silicate Weight Ratio	Number of Cracked Samples Per 10 Samples
1 day at 60°C 1 day at 105°C	50:50	10
2 days at 60°C	50:50	5
2 days at 50°C	50:50	2
2 days at 45°C	50:50	0
11 days at 22°C (Room Temp.)	50:50	0

Figure 4-5: Cracked wood-resin composite samples.

The amount of weight loss during the drying process was measured for both oven curing and room temperature curing. Figure 4-6 displays the average weight loss of each sample set for samples oven cured for two days at 45°C, and for samples cured at room temperature over eleven days. Each of these sample sets had a wood to resin weight ratio of 50:50 and used a wood element size of < 40 mesh. All samples had a total weight loss from drying between 35-40%.

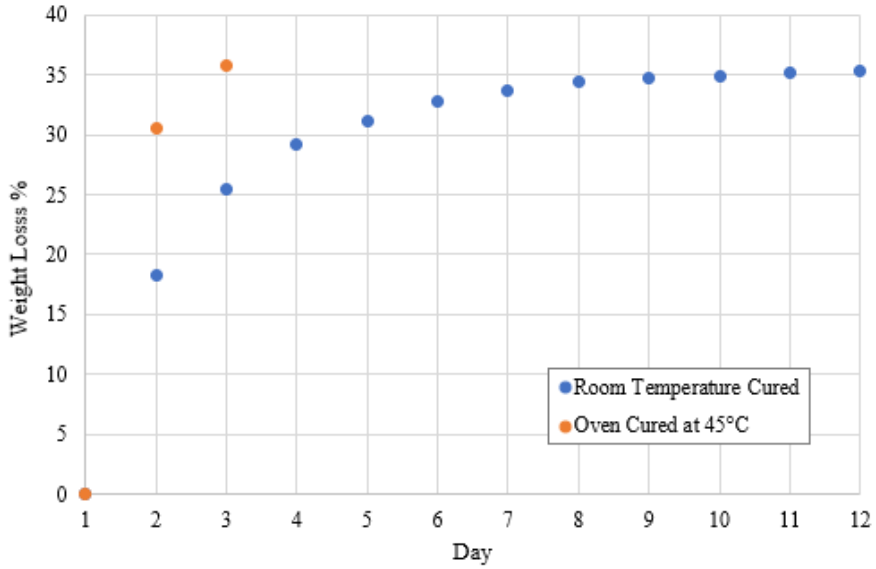

Figure 4-6: Sample weight loss during curing process.

4.2 Static Bend Testing

Once wood-resin composites were extruded and cured, their bending strength was tested using a 3-point static bending test. The wood to resin weight ratio, wood element size, and curing rate were the three parameters tested independently.

To test the effect of curing rate on the bending strength of the composite, five sample sets were cured using different methods. Each of these sample sets had a consistent wood to resin weight ratio of 50:50, and a consistent wood element size of < 40 mesh. Table 4-2 lists the five curing methods used. The average bend strength of each sample set is shown in Figure 4-7 and the average modulus of elasticity in bending for each sample set is shown in Figure 4-8.

Table 4-2: Curing methods.

Method #	Curing Method
1	2 days at 60°C
2	2 days at 50°C
3	2 days at 45°C
4	11 days 22°C (Room Temperature)
5	1 day at 60°C 1 day at 105°C

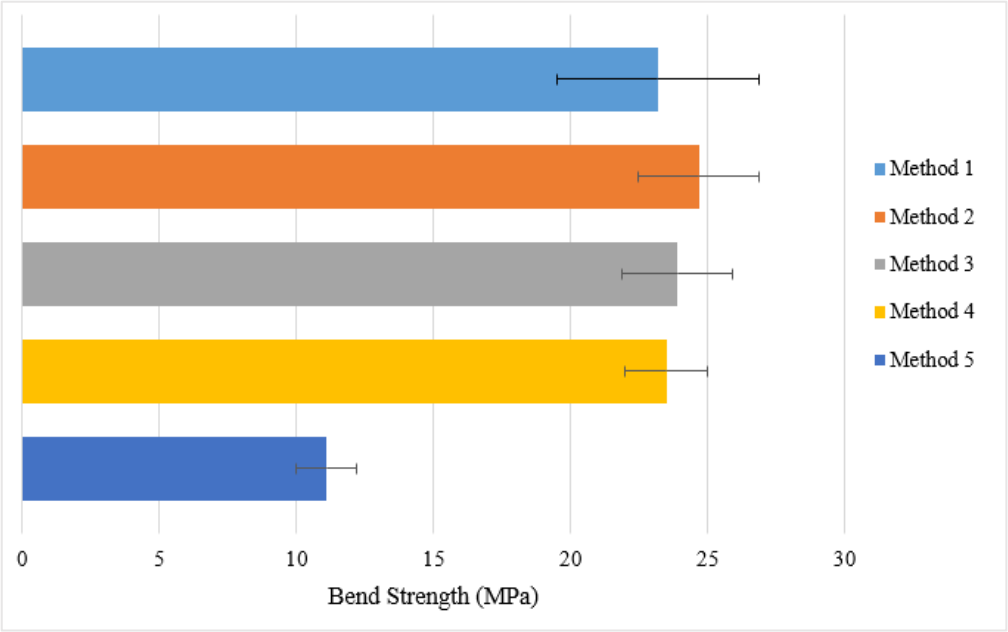

Figure 4-7: Bend strength of composites at varied curing rates.

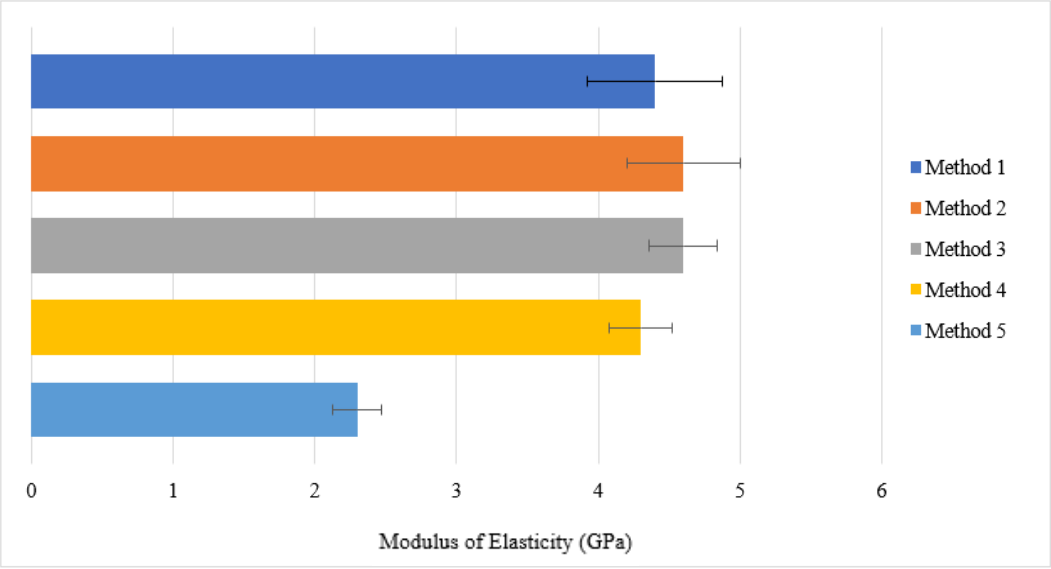

Figure 4-8: Modulus of elasticity of composites at varied curing rates.

Three sample sets of varied wood to resin weight ratios were tested using the 3-point bending method. Each of the three sample sets used the uniform curing method of oven curing for two days at 50°C. Additionally, the sample sets all used a wood element size of < 40 mesh. The average bend strength and modulus of elasticity of each sample set were determined and are shown in Figure 4-9 and Figure 4-10 respectively. Wood to resin weight ratios of 50:50, 55:45, and 60:40 were the three content ratios evaluated.

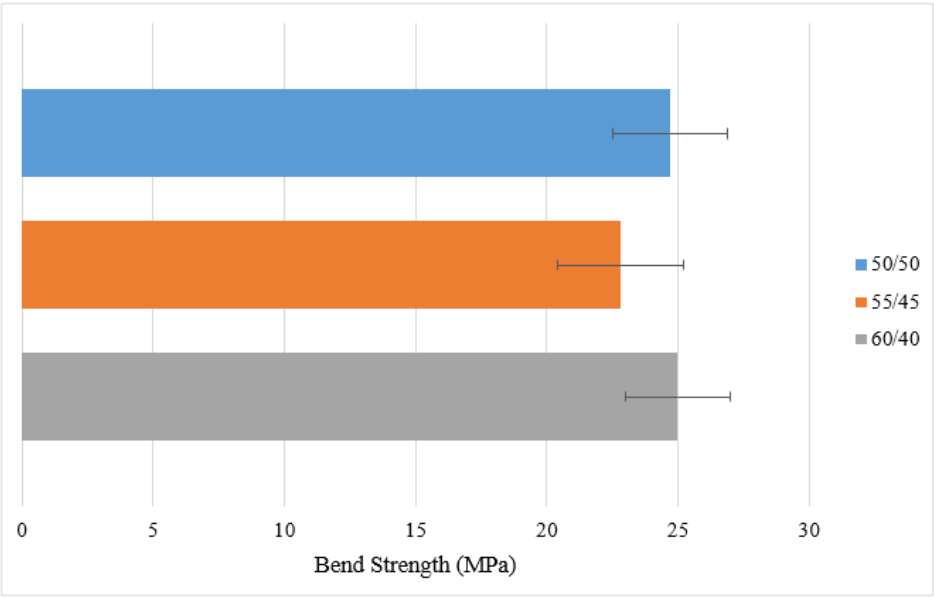

Figure 4-9: Bend strength of composites at varied wood to resin weight ratios.

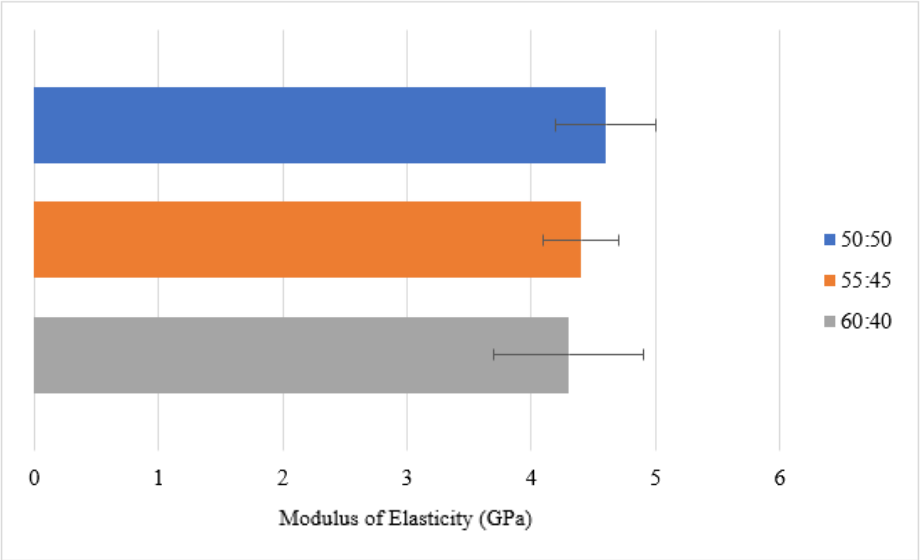

Figure 4-10: Modulus of elasticity of composites at varied wood to resin weight ratios.

A set of extruded samples were made using wood element size of 20-40 mesh. This was done to compare the effect of wood element size on strength and modulus of elasticity. However, as seen in Figure 4-3 these samples were extremely cracked and nonuniform. Due to the poor sample condition, the 3-point bending test results were inconsistent and unreliable. For example, Figure 4-11 compares a flexural stress vs. flexural strain curve of a sample with wood element size of 20-40 mesh to a stress vs. strain curve of a sample with wood element size of < 40 mesh. Flexural stresses and strains were calculated using equations 16 and 17, respectively.

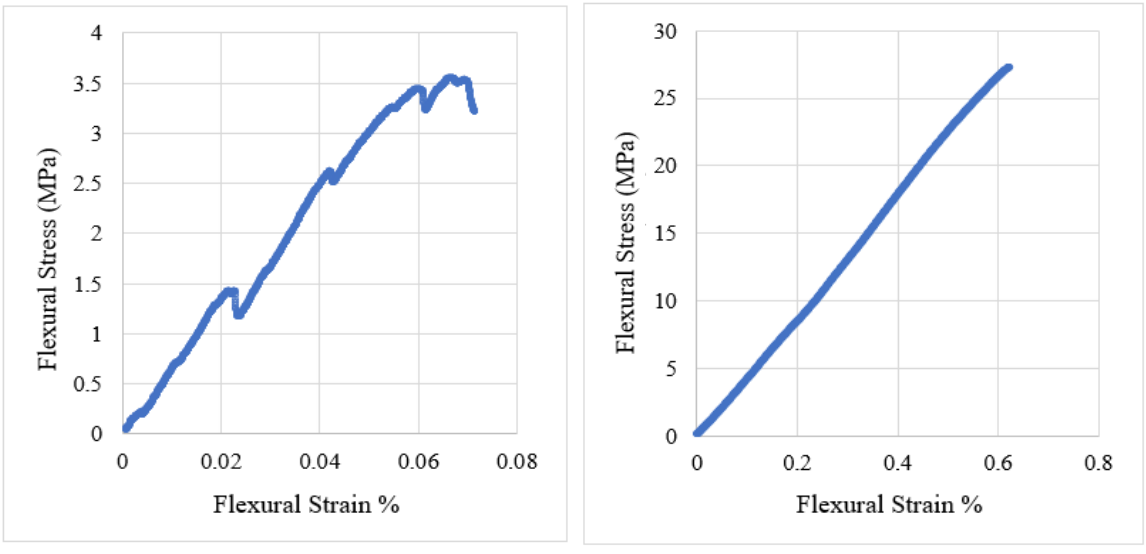

Figure 4-11: Stress vs. strain curve of 20-40 mesh sample (left),
stress vs. strain curve of < 40 mesh sample (right).

4.3 Viscosity Model

4.3.1 Experimental Results

Using the method described in Section 3.3.1, true viscosity and true shear rate of the wood-resin composite were calculated from the rheological data collected. The true viscosity is plotted as a function of true shear rate in Figure 4-12 on a log-log scale. Additionally, a Power-law fitted curve is used to model this function. This data includes both capillary and dynamic rheology data. This composite had a wood to resin weight ratio of 50:50 and used a wood element size of < 40 mesh.

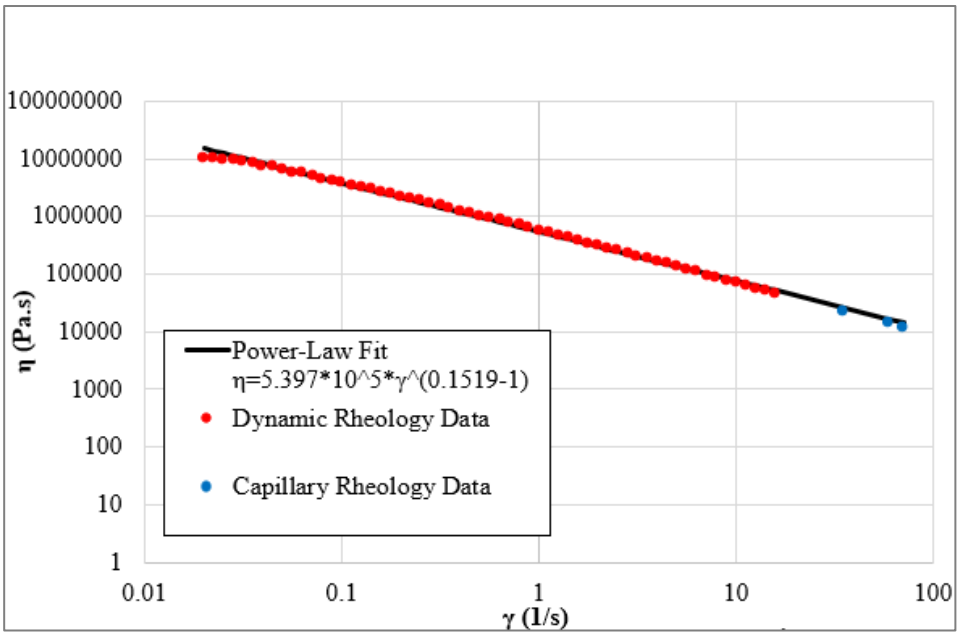

Figure 4-12: True viscosity vs. true shear rate of a wood-resin composite.

Figure 4-13 shows the load on the capillary crosshead as a function of compressive extension. This test was performed using the custom-built capillary rheometer and die described in Section 3.2. The crosshead speed was 0.1667 mm/s, and the wood-resin composite used a wood to resin weight ratio of 50:50, with wood element size of < 40 mesh. The compressive pressure at the critical extrusion point was 4.76 MPa. The density of the compressed composite was calculated to be 1250 kg/m^3. The data from this capillary extrusion can be used to compare to a CFD model.

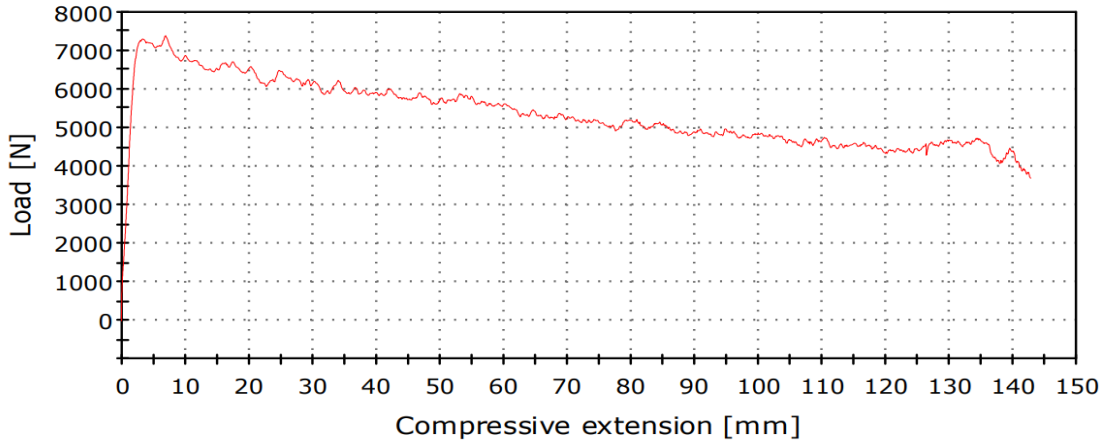

Figure 4-13: Capillary rheology data for a crosshead speed of 0.1667 mm/s.

4.3.2 CFD Results

A CFD study was performed to simulate the capillary rheology test described in Section 4.3.1. The simulation used the determined compressed composite density of 1250 kg/m^3 and used the Power-law viscosity model described in Equation 18. Further details of the simulation methods can be found in Section 3.3.2.

$$\eta = 5.397 \times 10^5 \, \dot{\gamma}^{0.1519-1} \tag{18}$$

The wall shear stress on the capillary barrel was unknown, thus three different boundary conditions were tested. The three boundary conditions were no-slip, specified shear stress of 100 Pa, and specified shear stress of 1000 Pa. A mesh element size of 2.5x10^{-4} m was used for these three simulations. Additionally, two other meshes were applied to the simulation with wall shear stress of 1000 Pa. These two meshes had element sizes of 1x10^{-3} m, and 5x10^{-4} m. The simulated maximum pressure in the barrel at the time step of 0.5 s was used to compare to the experimental critical extrusion pressure. Figure 4-14 is the pressure contours inside the barrel at 0.5 s using a specified wall shear stress of 1000 Pa and mesh element size of 2.5x10^{-4} m. The maximum pressure in this simulation is 4.84 MPa.

Figure 4-14: Pressure contour with a specified wall shear stress of 1000 Pa.

Table 4-3 contains the simulation results for the three simulations with varied wall boundary conditions, as well as the two simulations with varied mesh element size.

Table 4-3: CFD simulation results.

Wall Boundary Condition	**Mesh Element Size (m)**	**Extrusion Pressure (MPa)**
No-slip	$2.5x10^{-4}$	21.8
100 Pa	$2.5x10^{-4}$	3.58
1000 Pa	$2.5x10^{-4}$	4.84
1000 Pa	$5x10^{-4}$	2.59
1000 Pa	$1x10^{-3}$	2.51

Chapter 5: Discussion and Analysis

5.1 Wood Composite Screw Extrusion

In order to extrude the wood-based composite effectively, many advancements and modifications were made to the screw extrusion method. These include die modifications, motor improvements, specialized screws, and changes to the wood-resin composite. Many observations were made throughout this process on what parameters effect the extrusion performance. The following is a list of these observations:

- The wood to resin ratio greatly effects the extrudability of the composite. Without enough resin and water, the composite can become too dry and is difficult to extrude. Additionally, dry extrudate is flaky, less malleable, and exhibits the sharkskin effect more often.
- Larger wood elements of size greater than 40 mesh tend to have more obstacles extruding than wood elements of size less than 40 mesh. More pressure is required to extrude these elements and composites made from larger wood elements tend to experience more die swell.
- High compression ratio screws are not suitable for extruding wood-based composites. These screws cause unnecessary friction between the wood and the barrel. This can result in motor stalling and overheating. Composites with high wood content experience this issue most. Thus, it is better to use a screw with low or no compression ratio.
- Larger die diameters make extruding the composite easier. The larger the die, the less pressure is required to extrude. However, the resulting composite will be less dense.

During the screw extrusion, the primary wood composite issue was the sharkskin effect. Initially, when using the screw extruder, the sharkskin effect occurred often. It was especially present when extruding at high shear rates. However, after using the screw extruder for numerus extrusions, the composite no longer experienced the sharkskin effect. Sharkskin is thought to be caused by the stick-slip phenomenon and occurs in the die. It occurs when a critical shear stress and a critical acceleration are met [26]. Die swell is a phenomenon in which the extrudate expands after existing the die. It occurs because as the extrude leaves the die all added pressure is removed and the material relaxes [22]. At high flow rates die swell is common and can attribute to the sharkskin effect. Die swell was often present during extrusions which experienced sharkskin. The die used with the screw extruder originally had a rough inside surface, which causes increased shear stress. The composite likely stopped experiencing sharkskin effect due to the die surface becoming smoother from wear.

5.2 Wood Composite Properties

Some of the composite samples experienced surface cracking during the curing process. Table 4-1 lists the number of cracked samples per ten samples for various curing methods. The curing method which resulted in the most cracked samples was oven curing the samples for one day at 60°C and one day at 105°C. Every wood composite sample cracked during this method. Two curing methods experienced no surface cracking. These were oven curing for two days at 45°C and curing at room temperature. It appears that curing the composites at higher temperatures resulted in more surface cracking. Additionally, these cracks were often longer and wider. The cracking likely occurred due to a thermal differential and the large amount of water being rapidly evaporated through the surface. All samples experienced a weight between 35-40% during the curing process from water loss. The largest amount of weight loss occurred in samples cured at the highest temperatures. As seen in Figure 4-6, the rate at which the samples dried differed from oven curing and room temperature curing.

As seen in Figure 4-7 and Figure 4-8, the bending strength and modulus of elasticity in bending of the composite samples did not seem to be affected by the curing method used, except for the samples cured for one day at 60°C and one day at 105°C (Method 5). A Student t-test was used analyze the statistical significance of the data. This was done by comparing the bending strength data of each curing method to curing Method 1. For methods 2, 3, and 4 the significance levels (p) were 0.35, 0.67, and 0.86, respectively. Since all these methods have $p > 0.05$ there is no significant difference in their result compared to Method 1. Method 5 had a p-value of 1.49×10^{-5}, meaning that there is a significant difference between curing Method 5 and 1. It is likely that these samples had lower bending strength and a lower modulus of elasticity because they all were severely cracked. Similarly, the wood to resin weight ratio did not appear to affect the bending strength and modulus of elasticity of the composite samples. As seen in Figure 4-9 and 4-10, the bending properties of all three sample sets are reasonably close. A t-test was used to compare the bending strength data of the 55:45, and 60:40 ratio samples to the 50:50 ratio samples. The p-values for the 55:45, and 60:40 data sets were 0.19 and 0.77 when compared to the 50:50 data set, thus there was no statistical significance between the data sets. However, the wood to resin weight ratios used are relatively similar. Using much higher or lower wood to resin weight ratio could result in different bending properties. Unfortunately, the composite samples with wood element size of 20-40 mesh did not extrude well. These samples suffered a large amount of die swell and were very fragile. On average their diameters swelled 0.3 cm after extruding. Figure 4-11 compares a stress vs. strain curve of one of these samples

to a sample with wood element size of < 40 mesh. The composite with larger element size had a very uneven stress curve and unreliable results.

Compared to the industry standard wood-based composites, the extruded composites had relatively the same density as medium-density fiberboard. The average bending strength of the composites with wood element size of < 40 mesh, which were cured for two days at 50°C, was 24.7 MPa. When compared to the composites in Table 2-1, this is less than medium-density fiber board, but greater than particle board. The modulus of elasticity of this extruded composite is 4.6 GPa, which is greater than both medium-density fiber board and particle board. Overall, this extruded composite has competitive properties when compared to industry leading wood-based composites.

5.3 Viscosity Model

The data used in Figure 4-12 came from dynamic and capillary rheology experiments on the same wood composite. Capillary rheology provided data for higher shear rates, while the dynamic rheology was done at lower shear rates. This gave a large range of shear rate values. Non-Newtonian fluids are those which have their viscosity dependent on shear rate. Thus, this wood composite can be classified as non-Newtonian. Since the viscosity of this composite lowers as shear rate increases, it is known as a shear-thinning material. This viscosity behavior is similar to paper pulp, while materials such as starch solutions are shear-thickening [27]. Figure 5-1 illustrates the behavior of a shear thinning material. In contrast to Figure 4-12, this curve has two non-linear sections, as well as the η_o and η_∞ values. Figure 4-12 does not have these features because all the experiments performed were in the linear region of the viscosity vs. shear rate curve.

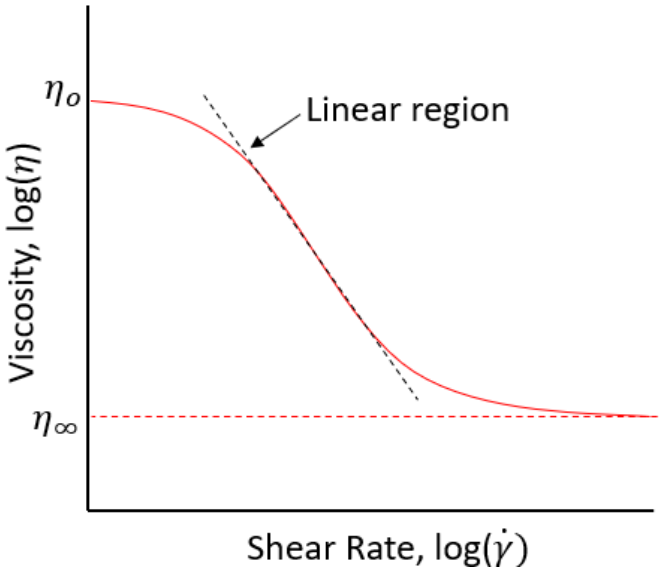

Figure 5-1: Shear thinning behavior.

As seen in Equation 15, a power-law model is a common model to characterize non-Newtonian fluids. The power-law model used to characterize the wood composite is Equation 18. In this model $n = 0.1519$, therefor $n < 1$. This indicates that the fluid is shear-thinning. If $n = 1$ the fluid would be a Newtonian fluid and if $n > 1$ the fluid would be shear-thickening.

The power-law model was chosen over other viscosity models because it is a versatile non-Newtonian model easily used in CFD. The Carreau-Yasuda is another model, which could have been used, but it is only used for shear-thinning viscosity behavior and initially the type of non-Newtonian

behavior was unknown. The Cross model is another common viscosity model however, it is commonly used to describe low-shear-rate behavior [28, 29].

5.4 CFD Simulation

When using a mesh element size of $2.5x10^{-4}$ m and a wall shear stress value of 1000 Pa, the CFD model simulated a critical extrusion pressure of 4.84 MPa. This was modeled after a capillary rheology extrusion with an experimental critical extrusion pressure of 4.76 MPa. Thus, using Equation 19 the percent error between the model and the experimental results is 1.6%.

$$error\ \% = \frac{|simulation\ result - \ experimental\ result|}{experimental\ result} \tag{19}$$

However, for the simulations which used different mesh element sizes or different wall shear stress values the error is much larger. As seen in Table 4-3, the simulated extrusion pressure when using a mesh element size of $1x10^{-3}$ m was 2.51 MPa, and when using a mesh element size of $5x10^{-4}$ m the extrusion pressure was 2.59 MPa. Thus, as the mesh becomes more refined the resulting extrusion pressure increases.

While the critical extrusion pressure was simulated accurately with the CFD model, the entire extrusion was not simulated. To further validate this model, the CFD simulation could be ran for a longer time duration. Results from multiple time-steps could then be compared to the experimental results.

Chapter 6: Summary and Conclusions

6.1 Summary

Additive manufacturing is expanding rapidly in the construction building industry. Applying additive manufacturing in construction can reduce waste and produce geometries that could not be produced with other manufacturing methods. Currently, concrete is the primary material being used in these applications. Wood-based composites are a cornerstone in the construction industry, but a practical method to produce them with additive manufacturing has yet to be fully developed. In the construction industry, wood-based composites typically have a high wood content to reduce cost. However, high wood content composites are difficult to produce with traditional additive manufacturing processes.

To solve the problems wood-based composites face when attempting to use them in conventional additive manufacturing processes, a new method has been developed. This method utilizes screw extrusion to provide a continuous material flow.

Understanding the properties of the wood-based composite is critical to its use in additive manufacturing. Utilizing a thermoset resin as the composite's adhesive allows the composite to extrude in a semi-fluid state while still hardening afterwards into a strong construction material. Capillary rheology and CFD are two powerful tools that can be applied to analyze the viscosity of a wood-based composite. Once a wood-resin composite is cured, the mechanical properties can be evaluated by using a 3-point bending test.

This study discusses the design and implementation of a custom capillary rheometer and a wood composite screw extruder. The purpose of developing a screw extruder was for its use in additive manufacturing. The flow properties of the wood-based composite were analyzed during extrusion and the mechanical properties were tested once the composite had cured. Sodium silicate was the resin used in the composite. Various parameters of the composite were tested, including wood to resin ratio, wood element size, and curing method. A CFD model of the capillary rheometer was made to aid in modelling the viscosity of the composite.

6.2 Conclusions

Because screw extrusion has typically been used for plastic melts, standard screw extruders do not have the capabilities to extrude a wood-based composite with high wood content. Thus, a screw extruder had to be designed and produced with the capabilities to extrude a wood composite. To extrude a wood-based composite with high wood content, the screw extruder must have a more powerful motor than a traditional plastic screw extruder. Additionally, the extruder will perform best while using a screw with no compression ratio. The wood-based composite flows best when it used small wood elements. Typically, the higher the resin and water content of composite the easier it is to extrude, but more expensive.

It was discovered that unless sever cracking occurred, the curing method did not greatly affect the mechanical properties of the composite. The strongest samples produced were those with wood element size < 40 mesh and cured for two days at 50°C. These samples had a bending strength of 24.7 MPa and a modulus of elasticity of 4.6 GPa. Since curing temperature did not affect the results, curing should be performed at room temperature to reduce energy consumption costs. These mechanical properties are relatively close to industry leading wood-based composites, such as OSB and fiber board. Thus, the extruded wood-based composites are suitable to replace traditional composites based on strength and modulus performance.

To gain a better understanding of how the composited flowed during extrusion, a custom capillary rheometer was designed and fabricated. Using this capillary rheometer experiments were conducted, and the viscosity of the composite was modeling using the power-law model. A CFD model was implemented to simulate the capillary extrusion. This model was able to simulate the critical extrusion pressure with an error of 1.6%. It was concluded that the power-law model was a suitable viscosity model to apply based on the CFD results.

Chapter 7: Future Work

The purpose of this research is to develop a reliable process for 3D printing house walls, floors, and roofs on a horizontal printing bed using a wood-based composite. Wood is a sustainable, environmentally friendly building resource. If a construction additive manufacturing method were developed using a wood-based composite it could greatly reduce construction costs and energy usage.

Future work using the screw extrusion process should entail implementing the system with a large-scale 3D printer. Once a functional wood-based composite 3D printer is developed, large scale composite prints should be made and tested. During the 3D printing process and rectangular die could be used to allow for layering of the material. Further exploration into curing the composite should be performed. Sodium silicate can be cured using CO_2 injection, this process could result in different material properties and should be studied as a means of improving the mechanical properties and streamline manufacturing. The study of the effect of mesh size on the material properties should be continued, including using a wood element size smaller than < 40 mesh to determine which element size is optimal. The CFD model should be developed further for the capillary rheometer by using particle-based flow simulations such as Ansys Polyflow or Rocky DEM. Additionally, a CFD model of the screw extrusion process should be made to aid in screw and die designs.

References

1. Newswire, P. *$1.5 Billion 3D Printing Construction Market, 2024 by Material Type (Concrete, Metal, Composite), Construction Method (Extrusion, Powder Bonding), End-Use Sector (Building, Infrastructure)*. 2019.
2. Delgado Camacho, D., et al., *Applications of additive manufacturing in the construction industry – A forward-looking review.* Automation in Construction, 2018. **89**: p. 110-119.
3. Tingjie Li*, J.A., Arlene Kingsland, Lyne M. Cormier, Xuejun Zou, *3D Printing – A Review of Technologies, Markets, and Opportunities for the Forest Industry.* Journal of Science & Technology for Forest Products and Processes, 2016. **5**.
4. Ayrilmis, N., *Effect of layer thickness on surface properties of 3D printed materials produced from wood flour/PLA filament.* Polymer Testing, 2018. **71**: p. 163-166.
5. Henke, K., et al., *Individual layer fabrication (ILF): a novel approach to additive manufacturing by the use of wood.* European Journal of Wood and Wood Products, 2021. **79**(3): p. 745-748.
6. Kalpakjian, S.S., Steven, *Manufacturing Processes for Engineering Materials* 6th ed. 2017: Pearson.
7. Mani, M., et al., *Measurement Science Needs for Real-time Control of Additive Manufacturing Powder Bed Fusion Processes*. 2015, U.S. Dept. of Commerce, National Institute of Standards and Technology.
8. Ayrilmis, N., *Effect of layer thickness on surface properties of 3D printed materials produced from wood flour/PLA filament.* Polymer Testing, 2018. **71**: p. 163-166.
9. Salas-Bringas, C.L., Odd-Ivar, *Development of a New Capillary Rheometer that uses Direct Pressure Measurements in the Capillary.* Nordic Rheology Society. **17**.
10. Li, T.Q. and M.P. Wolcott, *Rheology of HDPE–wood composites. I. Steady state shear and extensional flow.* Composites Part A: Applied Science and Manufacturing, 2004. **35**(3): p. 303-311.
11. Coogan, T.J. and D.O. Kazmer, *In-line rheological monitoring of fused deposition modeling.* Journal of Rheology, 2019. **63**(1): p. 141-155.
12. Haguija, N., *Application of Computational Fluid Dynamics to Design of Polymer Extrusion Dies*, in *TSME-International Conference on Mechanical Engineering*. OP Publishing.
13. Chhanwal, N., et al., *Computational Fluid Dynamics (CFD) Modeling for Bread Baking Process—A Review.* Food and Bioprocess Technology, 2012. **5**(4): p. 1157-1172.
14. Ramachandran, R.P., et al., *Computational Fluid Dynamics in Drying Process Modelling—a Technical Review.* Food and Bioprocess Technology, 2017. **11**(2): p. 271-292.

15. Sanderse, B., S.P. Pijl, and B. Koren, *Review of computational fluid dynamics for wind turbine wake aerodynamics.* Wind Energy, 2011. **14**(7): p. 799-819.
16. *ANSYS Fluent 12.0 User's Guide*.
17. (U.S.), F.P.L., *Wood Handbook*. 2010: U.S. Dept. of Agriculture, Forest Service, Forest Products Laboratory.
18. Chhanwal, N., et al., *Computational Fluid Dynamics (CFD) Modeling for Bread Baking Process—A Review.* Food and Bioprocess Technology, 2012. **5**(4): p. 1157-1172.
19. Wilczyński, A. and M. Kociszewski, *Bending properties of particleboard and MDF layers.* Holzforschung, 2007. **61**(6): p. 717-722.
20. Bekhta, P. and R. Marutzky, *Bending strength and modulus of elasticity of particleboards at various temperatures.* Holz als Roh- und Werkstoff, 2006. **65**(2): p. 163-165.
21. Starkm, N.M.G., D.J., *Outdoor durability of wood±polymer composites*, in *Wood-Polymer Composites*. 2008, Woodhead Publishing
22. Batchelor, B.H., *Physics of Plastics*. 1992: Hanser.
23. White, J.P., Helmut, *Screw Extrusion*. 1991: Hanser.
24. Hoffmann, M., et al., *Automation in the Construction of a 3D-Printed Concrete Wall with the Use of a Lintel Gripper*. Materials (Basel), 2020. **13**(8).
25. ASTM, *ASTM D3835 Standard Test Method for Determination of Properties of Polymeric Materials by Means of a Capillary Rheometer*.
26. Vlachopoulos, J.S., D., *Rheology of Molten Polymers*, in *Multilayer Flexible Packaging*. 2016, Plastics Design Library. p. 77-96.
27. Levenspiel, O., *Engineering flow and heat exchange*. 1998: Plenum Press.
28. Cui, Lu., et al., *Rheology of PLA/regenerated cellulose nanocomposites prepared by the pickering emulsion process: Network formation and modeling.* Materials & design, 2021. 206, p.109774.
29. MIT.edu., *Viscosity Models.* 2017 https://abaqus-docs.mit.edu/2017/English/SIMACAEMATRefMap/simamat-c-viscosity.htm#:~:text=The%20power%20law%20model%20is%20commonly%20used%20to,%3B%20%CE%B7%20min%20%E2%89%A4%20%CE%B7%20%E2%89%A4%20%CE%B7%20max%2C

Appendix A – Screw Design

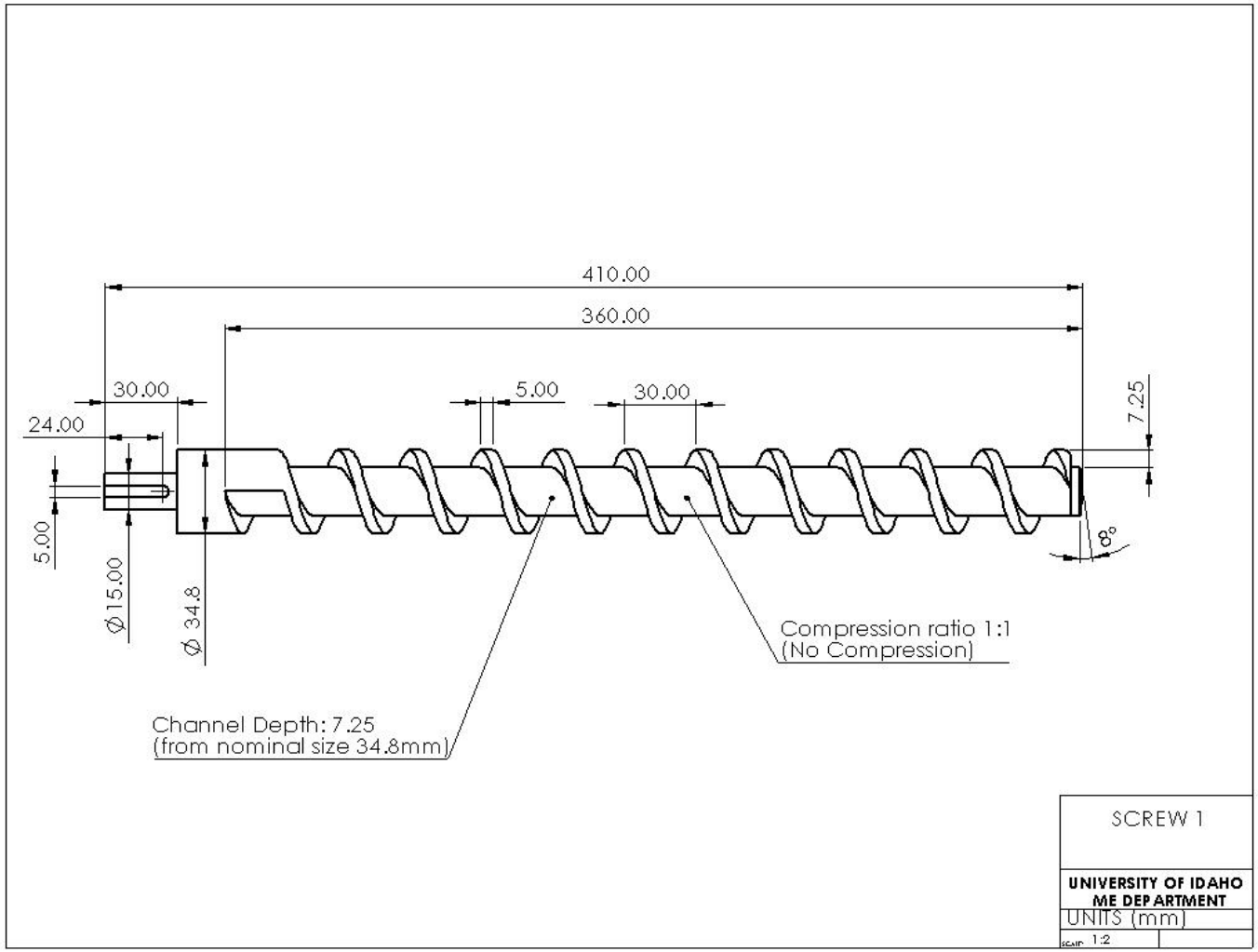

Appendix B – Capillary Rheometer Design

ITEM NO.	PART NUMBER	DESCRIPTION	QTY.
1	Bottom_Plate_NO_BUILD		1
2	Leg		4
3	Top_Plate		1
4	3314N27		4
5	91251A716		4
6	BarrelASM		1
7	Plunger		1

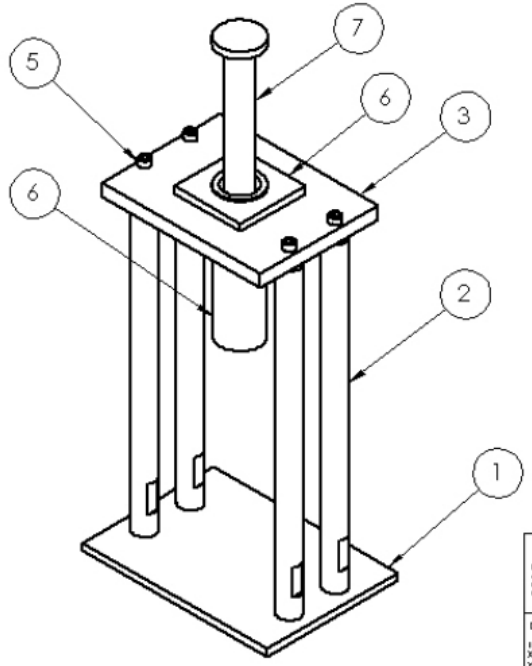

PROPRIETARY AND CONFIDENTIAL
THE INFORMATION CONTAINED IN THE DRAWING IS THE SOLE PROPERTY OF UNIVERSITY OF IDAHO ME DEPARTMENT. ANY REPRODUCTION IN PART OR AS A WHOLE WITHOUT THE WRITTEN PERMISSION OF UNIVERSITY OF IDAHO ME DEPARTMENT IS PROHIBITED.

DIMENSIONS ARE IN INCHES
THIRD ANGLE PROJECTION

MATERIAL:

DEFAULT TOLERANCES:
LINEAR: X ± .25, XX ± .1, XXX ± .01, XXXX ± .002
ANGULAR: X ± 2, XX ± 1, XXX ± 0.30'

DESCRIPTION:
CREATED BY: XXXXXXXXXX DATE: XX/XX/XX
DRAWN BY: DATE: 4/21/2021
FILENAME: Frame.SLDPRT

UNIVERSITY OF IDAHO
ME DEPARTMENT
PART #: QTY:
SCALE: 1:7 SHEET: 1 OF 1

ITEM NO.	PART NUMBER	QTY.
1	Weld_Plate	1
2	Barrel	1
3	End_Cap	1
4	91251A199	4

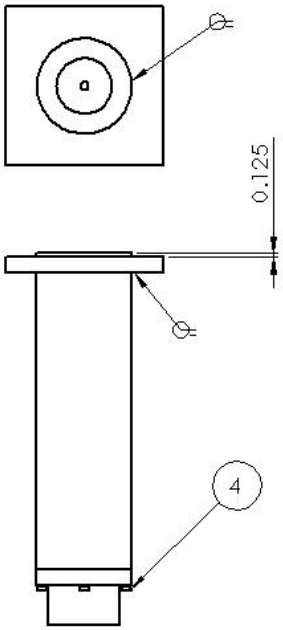

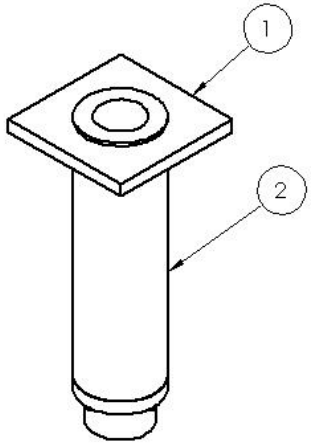

PROPRIETARY AND CONFIDENTIAL
THE INFORMATION CONTAINED IN THIS DRAWING IS THE SOLE PROPERTY OF UNIVERSITY OF IDAHO ME DEPARTMENT. ANY REPRODUCTION IN PART OR AS A WHOLE WITHOUT THE WRITTEN PERMISSION OF UNIVERSITY OF IDAHO ME DEPARTMENT IS PROHIBITED.

DIMENSIONS ARE IN INCHES
THIRD ANGLE PROJECTION

MATERIAL:

DEFAULT TOLERANCES:
LINEAR: X ± .25, XX ± .1, XXX ± .01, XXXX ± .002
ANGULAR: X ± 2, XX ± 1, XXX ± 0.30

DESCRIPTION:

CREATED BY: XXXXXXXXXX DATE: XX/XX/XX

DRAWN BY: DATE: 4/8/2020

FILENAME: BarrelASM.SLDPRT

UNIVERSITY OF IDAHO
ME DEPARTMENT

PART #: QTY:

SCALE: 1:4 SHEET: 1 OF 1

ITEM NO.	PART NUMBER	QTY.
1	Barrel	1

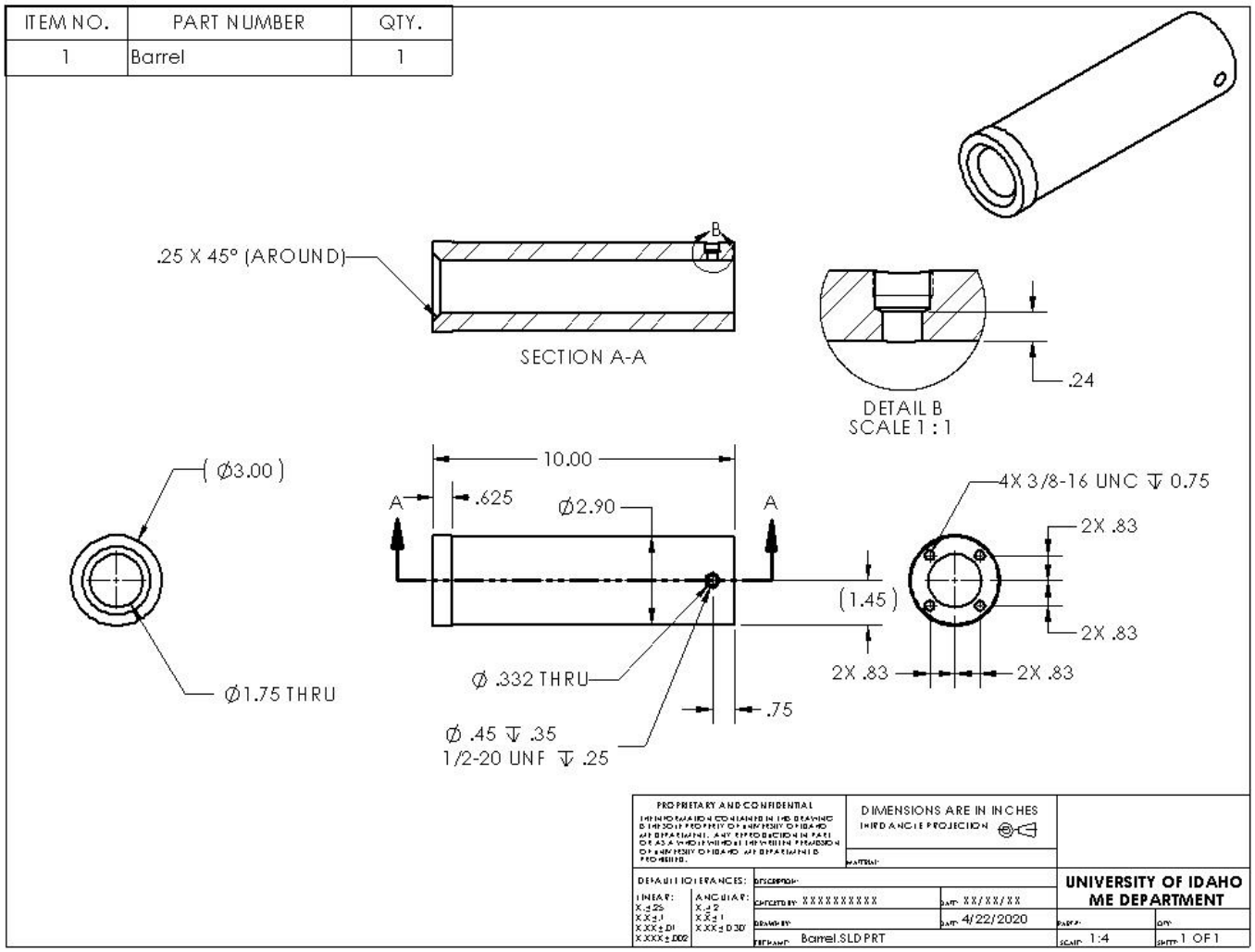

PROPRIETARY AND CONFIDENTIAL
THE INFORMATION CONTAINED IN THIS DRAWING IS THE SOLE PROPERTY OF UNIVERSITY OF IDAHO ME DEPARTMENT. ANY REPRODUCTION IN PART OR AS A WHOLE WITHOUT THE WRITTEN PERMISSION OF UNIVERSITY OF IDAHO ME DEPARTMENT IS PROHIBITED.

DIMENSIONS ARE IN INCHES
THIRD ANGLE PROJECTION

MATERIAL:

DEFAULT TOLERANCES:
LINEAR: X ± .25, XX ± .1, XXX ± .01, XXXX ± .0002
ANGULAR: X ± 2, XX ± 1, XXX ± 0.30

DESCRIPTION:
CREATED BY: XXXXXXXXXX DATE: XX/XX/XX
DRAWN BY: DATE: 4/22/2020
FILENAME: Barrel.SLDPRT

UNIVERSITY OF IDAHO
ME DEPARTMENT

SIZE: | QTY:
SCALE: 1:4 | SHEET 1 OF 1

ITEM NO.	PART NUMBER	QTY.
1	Plunger	1

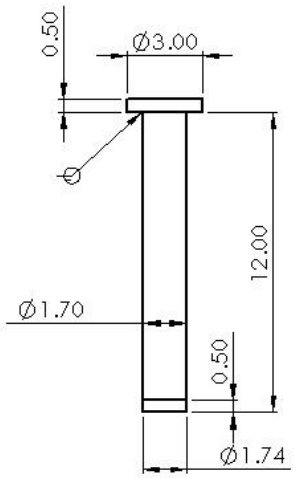

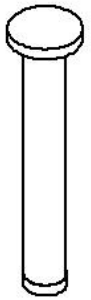

PROPRIETARY AND CONFIDENTIAL
THE INFORMATION CONTAINED IN THIS DRAWING IS THE SOLE PROPERTY OF UNIVERSITY OF IDAHO ME DEPARTMENT. ANY REPRODUCTION IN PART OR AS A WHOLE WITHOUT THE WRITTEN PERMISSION OF UNIVERSITY OF IDAHO ME DEPARTMENT IS PROHIBITED.

DIMENSIONS ARE IN INCHES
THIRD ANGLE PROJECTION

MATERIAL:

DEFAULT TOLERANCES:
LINEAR: X ± 25, XX ± .1, XXX ± .01, XXXX ± .002
ANGULAR: X ± 2, XX ± 1, XXX ± 0.30'

DESCRIPTION:

CHECKED BY: XXXXXXXXXX DATE: XX/XX/XX

DRAWN BY: DATE: 4/17/2020

DETAIL: Plunger.SLDPRT

UNIVERSITY OF IDAHO
ME DEPARTMENT

PART #: QTY:

SCALE: 1:5 SHEET: 1 OF 1

ITEM NO.	PART NUMBER	QTY.
1	Top_Plate	1

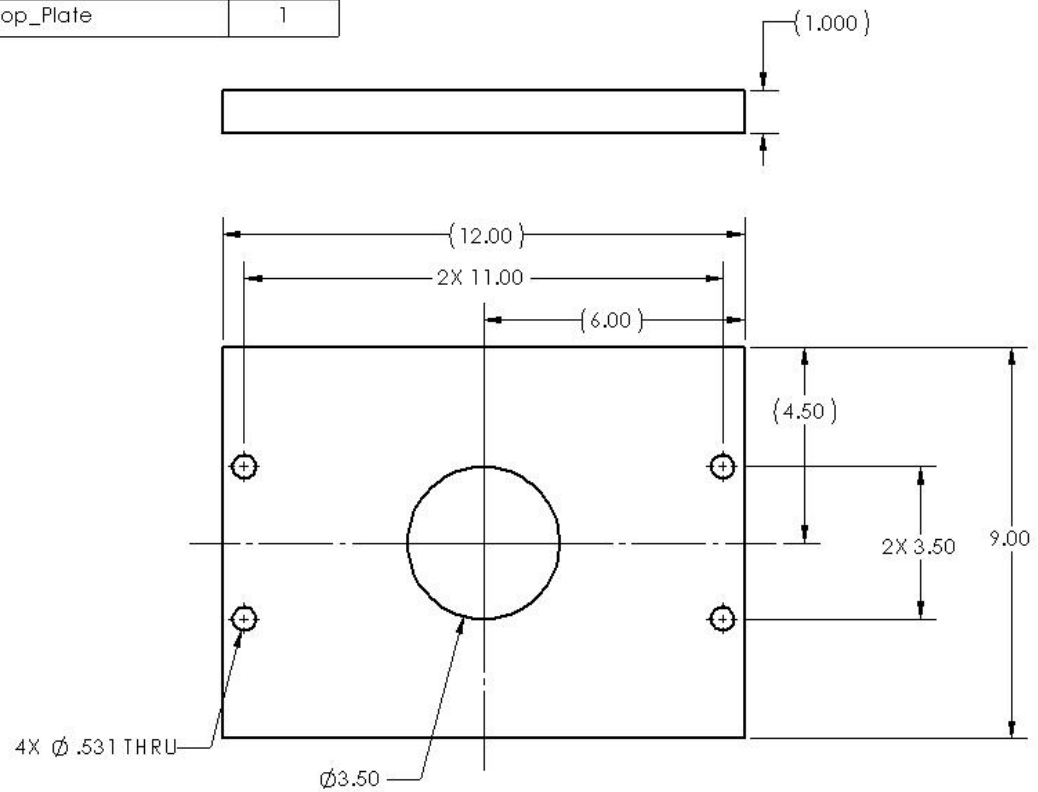

PROPRIETARY AND CONFIDENTIAL
INFORMATION CONTAINED IN THIS DRAWING IS THE SOLE PROPERTY OF UNIVERSITY OF IDAHO ME DEPARTMENT. ANY REPRODUCTION IN PART OR AS A WHOLE WITHOUT THE WRITTEN PERMISSION OF UNIVERSITY OF IDAHO ME DEPARTMENT IS PROHIBITED.

DIMENSIONS ARE IN INCHES
THIRD ANGLE PROJECTION

MATERIAL:

DEFAULT TOLERANCES:
LINEAR: X ± .25, XX ± .1, XXX ± .01, XXXX ± .0002
ANGULAR: X ± 2, XX ± 1, XXX ± 0.30

DESCRIPTION:
CREATED BY: XXXXXXXXXX DATE: XX/XX/XX
DRAWN BY: DATE: 3/31/2020
FILENAME: Top_Plate.SLDPRT

UNIVERSITY OF IDAHO
ME DEPARTMENT

PART #: QTY:
SCALE: 1:3 SHEET 1 OF 1

ITEM NO.	PART NUMBER	QTY.
1	Weld_Plate	1

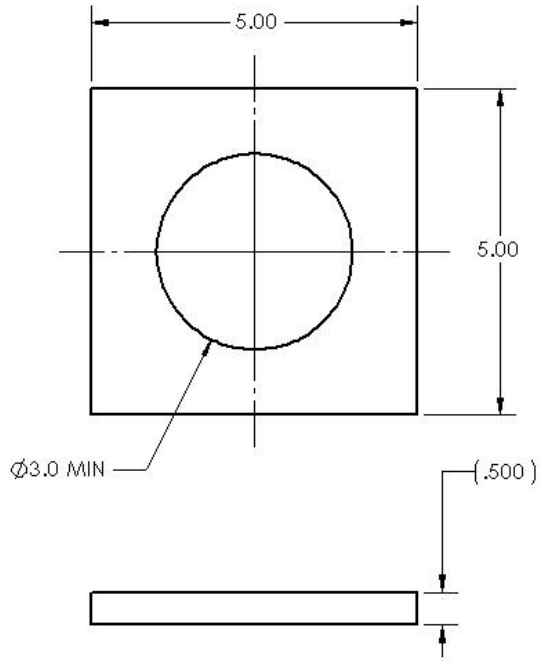

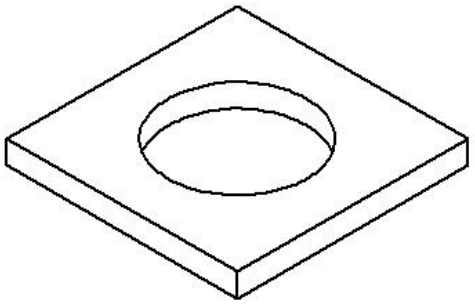

PROPRIETARY AND CONFIDENTIAL
INFORMATION CONTAINED IN THIS DRAWING IS THE SOLE PROPERTY OF UNIVERSITY OF IDAHO ME DEPARTMENT. ANY REPRODUCTION IN PART OR AS A WHOLE WITHOUT THE WRITTEN PERMISSION OF UNIVERSITY OF IDAHO ME DEPARTMENT IS PROHIBITED.

DIMENSIONS ARE IN INCHES
THIRD ANGLE PROJECTION

MATERIAL:

DEFAULT TOLERANCES:
LINEAR: X ± .25, XX ± .1, XXX ± .01, XXXX ± .0002
ANGULAR: X ± 2, XX ± 1, XXX ± 0.30

DESCRIPTION:
CREATED BY: XXXXXXXXXX DATE: XX/XX/XX
DRAWN BY: DATE: 3/29/2020
FILENAME: Weld_Plate.SLDPRT

UNIVERSITY OF IDAHO
ME DEPARTMENT

PART #: QTY:
SCALE: 1:2 SHEET 1 OF 1

ITEM NO.	PART NUMBER	QTY.
1	Leg	1

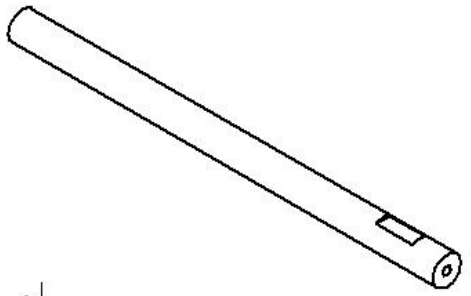

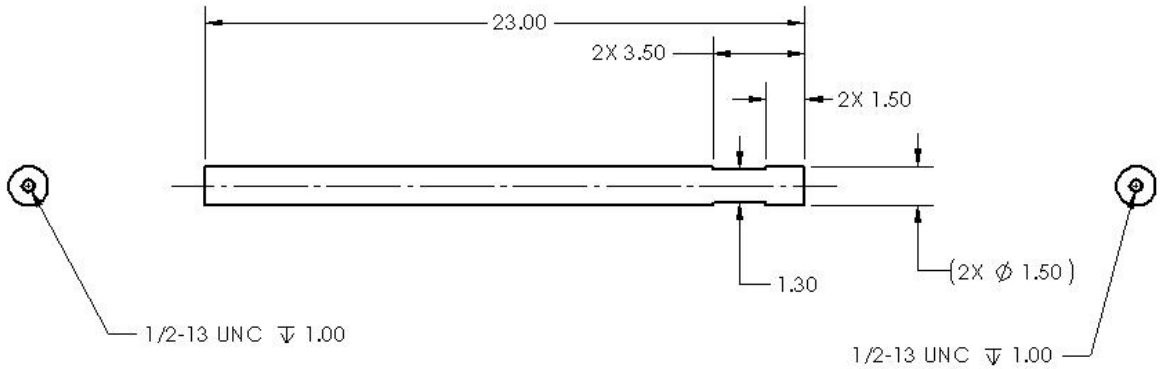

PROPRIETARY AND CONFIDENTIAL
THE INFORMATION CONTAINED IN THIS DRAWING IS THE SOLE PROPERTY OF UNIVERSITY OF IDAHO ME DEPARTMENT. ANY REPRODUCTION IN PART OR AS A WHOLE WITHOUT THE WRITTEN PERMISSION OF UNIVERSITY OF IDAHO ME DEPARTMENT IS PROHIBITED.

DIMENSIONS ARE IN INCHES
THIRD ANGLE PROJECTION

MATERIAL:

DEFAULT TOLERANCES:
LINEAR: X ± .25, XX ± .1, XXX ± .01, XXXX ± .0002
ANGULAR: X ± 2, XX ± 1, XXX ± 0.30

DESCRIPTION:
CREATED BY: XXXXXXXXXX DATE: XX/XX/XX
DRAWN BY: DATE: 3/29/2020
FILENAME: Leg.SLDPRT

UNIVERSITY OF IDAHO
ME DEPARTMENT

PART #: QTY:
SCALE: 1:5 SHEET 1 OF 1

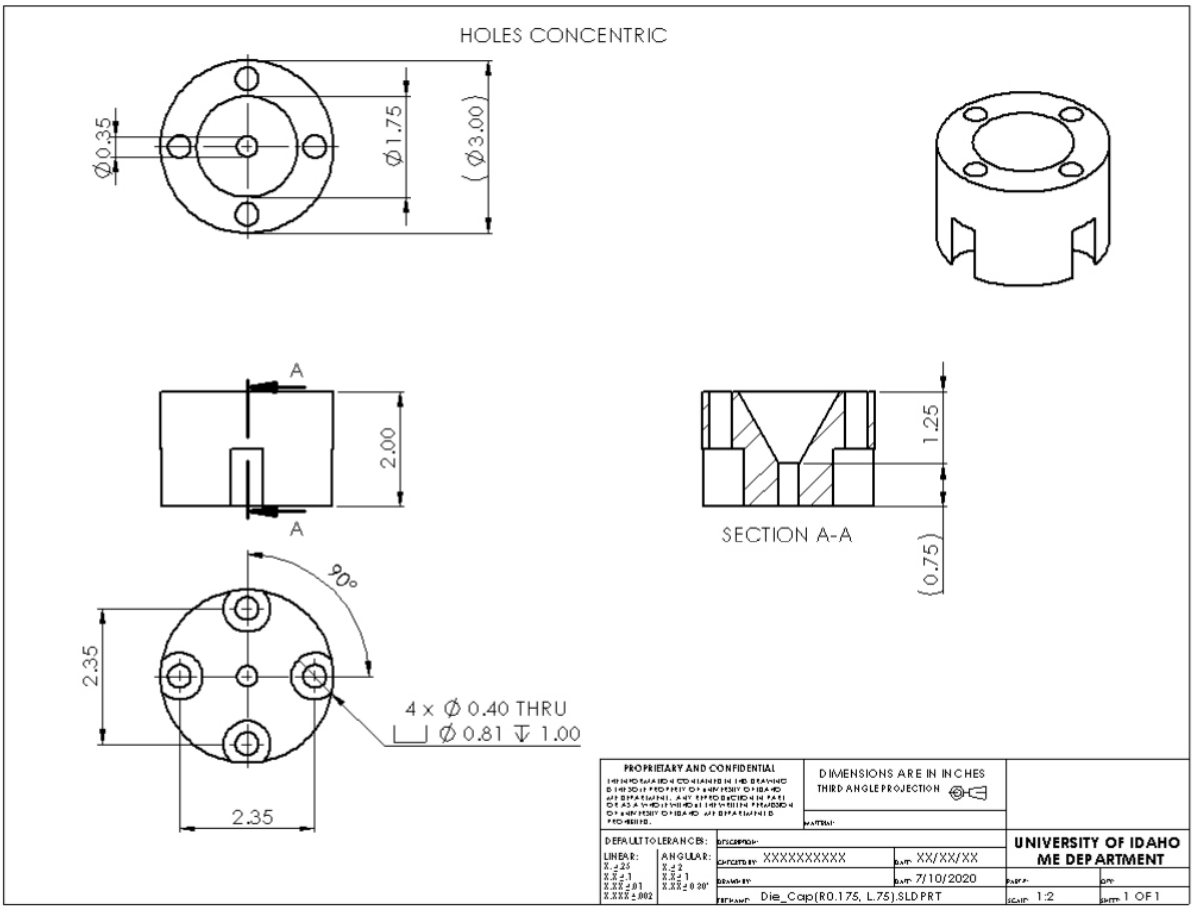
HOLES CONCENTRIC
Ø0.35
Ø1.75
(Ø3.00)
A
2.00
A
1.25
SECTION A-A
(0.75)
90°
2.35
4 x Ø 0.40 THRU
Ø 0.81 ↧ 1.00
2.35
PROPRIETARY AND CONFIDENTIAL
DIMENSIONS ARE IN INCHES
THIRD ANGLE PROJECTION
DEFAULT TOLERANCES:
LINEAR:
ANGULAR:
CREATED BY: XXXXXXXXXX
DATE: XX/XX/XX
DRAWN BY:
DATE: 7/10/2020
FILENAME: Die_Cap(R0.175, L.75).SLDPRT
UNIVERSITY OF IDAHO
ME DEPARTMENT
SCALE: 1:2
SHEET 1 OF 1